Earth and Planetary Science Letters
Manuscript Draft

Manuscript Number: EPSL-D-15-00011

Title: Fluid-related inclusions in Alpine high-pressure peridotite reveal trace element recycling during subduction-zone dehydration of serpentinized mantle (Cima di Gagnone, Swiss Alps)

Article Type: Letters

Keywords: Serpentinized mantle| Garnet peridotite |Chlorite harzburgite| Polyphase inclusions| Subduction fluids|Fluid-mobile elements

Abstract: The garnet metaperidotite and chlorite harzburgite bodies embedded in paragneisses in the tectonic mélange delineating the subduction interface at Cima di Gagnone are unique examples of ultramafic rocks that experienced multistage subduction metasomatism and devolatilization. Eclogite-facies olivine and garnet of garnet metaperidotite and chlorite harzburgite trap primary to pseudosecondary polyphase inclusions recording the fluid evolved during breakdown of antigorite and chlorite. Combined major element mapping and laser-ablation ICP-MS bulk inclusion analysis characterize the mineral composition of the polyphase inclusions and quantify the fluid chemistry. Silicates, Cl-bearing phases, sulfides, carbonates, and oxides document post-entrapment mineral growth starting immediately after fluid entrapment.
Compositional data reveal the presence of two different fluid types. The first type is hosted in olivine of the garnet metaperidotite and shows pronounced fluid-mobile and light rare earth element enrichments, with up to 103 PM (primitive mantle) Cl, Cs, Pb, As, Sb, ~102 PM Tl, Ba, while Rb, B, Sr, Li, U are of the order of 101 PM, and alkalis are ~2 PM. The second fluid type hosted by garnet and by olivine of the chlorite harzburgite is much less enriched in fluid-mobile elements but shows overall similar enrichment patterns. These data reveal a multistage fluid history affecting these peridotite lenses, including selective element enrichment during seafloor alteration followed by fluid rock interaction during subduction metamorphism along the plate interface. Here, sediment-equilibrated fluid infiltration produced serpentinized metaperidotites strongly enriched in fluid-mobile elements that were released again at greater depth upon dehydration. The fluid inclusions hosted by garnet may then record the composition of the chlorite breakdown fluid.
These data demonstrate that hydrous ultrabasic rocks may act as a sink and transporter of water and fluid-mobile element enrichments generated by both ocean floor hydration and fluid-mobile element enrichment via sediment equilibrated fluids during early subduction stages. Consequently, serpentinite devolatilization at subarc depths produces fluids enriched in crust and sediment-derived components to flux-melt the mantle wedge triggering arc magmatism, without the need of concomitant dehydration/melting of metasedimentary or altered oceanic crust lithologies.

Fluid-related inclusions in Alpine high-pressure peridotite reveal trace element recycling during subduction-zone dehydration of serpentinized mantle (Cima di Gagnone, Swiss Alps)

[1*]Marco Scambelluri, [2]Thomas Pettke, [1]Enrico Cannaò

[1]Dipartimento di Scienze della Terra, Ambiente e Vita, Università di Genova, Italy

[2] Institute of Geological Sciences, University of Bern, Switzerland

* Corresponding author: marco.scambelluri@dipteris.unige.it

Keywords: Serpentinized mantle, Garnet peridotite, Chlorite harzburgite, Polyphase inclusions, Subduction fluids, Fluid-mobile elements

Published in Earth and Planetary Science Letters 27 July 2015, Volume 429, P 45-59

http://dx.doi.org/10.1016/j.epsl.2015.07.060
Publisher version https://www.sciencedirect.com/science/article/pii/S0012821X15005038

Abstract

The garnet metaperidotite and chlorite harzburgite bodies embedded in paragneisses in the tectonic mélange delineating the subduction interface at Cima di Gagnone are unique examples of ultramafic rocks that experienced multistage subduction metasomatism and devolatilization. Eclogite-facies olivine and garnet of garnet metaperidotite and chlorite harzburgite trap primary to pseudosecondary polyphase inclusions recording the fluid evolved during breakdown of antigorite and chlorite. Combined major element mapping and laser-ablation ICP-MS bulk inclusion analysis characterize the mineral composition of the polyphase inclusions and quantify the fluid chemistry. Silicates, Cl-bearing phases, sulfides, carbonates, and oxides document post-entrapment mineral growth starting immediately after

fluid entrapment.

Compositional data reveal the presence of two different fluid types. The first type is hosted in olivine of the garnet metaperidotite and shows pronounced fluid-mobile and light rare earth element enrichments, with up to 10^3 PM (primitive mantle) Cl, Cs, Pb, As, Sb, $\sim 10^2$ PM Tl, Ba, while Rb, B, Sr, Li, U are of the order of 10^1 PM, and alkalis are $\sim$2 PM. The second fluid type hosted by garnet and by olivine of the chlorite harzburgite is much less enriched in fluid-mobile elements but shows overall similar enrichment patterns. These data reveal a multistage fluid history affecting these peridotite lenses, including selective element enrichment during seafloor alteration followed by fluid rock interaction during subduction metamorphism along the plate interface. Here, sediment-equilibrated fluid infiltration produced serpentinized metaperidotites strongly enriched in fluid-mobile elements that were released again at greater depth upon dehydration. The fluid inclusions hosted by garnet may then record the composition of the chlorite breakdown fluid.

These data demonstrate that hydrous ultrabasic rocks may act as a sink and transporter of water and fluid-mobile element enrichments generated by both ocean floor hydration and fluid-mobile element enrichment via sediment equilibrated fluids during early subduction stages. Consequently, serpentinite devolatilization at subarc depths produces fluids enriched in crust and sediment-derived components to flux-melt the mantle wedge triggering arc magmatism, without the need of concomitant dehydration/melting of metasedimentary or altered oceanic crust lithologies.

1. Introduction

Serpentinites trigger major tectonic and geochemical processes in Earth. Their abundance in oceanic plates and in subduction zones controls the water budgets and properties of slabs and

overlying mantle (Ulmer and Trommsdorff, 1995; Cannat et al., 1995; Iwamori, 1998; Rüpke et al., 2004; Frueh Green et al., 2004). Great importance is now given to the interface domains between subducting and overlying plates, where serpentinite forms kilometre-thick layers derived from hydration of supra-subduction mantle, or occurs in tectonic mélanges atop the slab, as matrix and as blocks of variable size and provenance (Bostock et al., 2002; Federico et al., 2007; Bebout, 2007). In such environments, the low viscosity and high water content of serpentinite control deformation focussing, fluid release and mass transfer (Gerya et al., 2003; Hyndman and Peacock, 2003; Bebout, 2007; Blanco-Quintero et al., 2011; Scambelluri et al., 2014). Several authors proposed that transfer of trace element-rich fluids from slab to mantle is dictated by serpentinite stability and by its capacity of storing water, carbon and fluid-mobile elements (Hattori and Guillot, 2003; Scambelluri et al., 2004a; Sharp and Barnes, 2004; Deschamps et al., 2010; 2011; 2013; Kendrick et al., 2011, 2013; John et al., 2011; Alt et al., 2013; Boschi et al., 2013; Shimizu et al., 2013; Evans et al., 2014; De Hoog et al., 2014). These elements are progressively extracted from serpentinite during the prograde dehydration reactions (1) antigorite + brucite = olivine + fluid, and (2) antigorite = olivine + orthopyroxene + fluid. Reaction (1) occurred in most eclogite-facies Alpine serpentinites, showing antigorite + olivine-bearing parageneses in rocks and in veins draining the released fluid (Plumper et al., 2014). The fluid is Cl-rich and contains variable amounts of B, Li (Scambelluri et al., 1997; 2004a; Scambelluri and Tonarini, 2012). A larger fluid amount is released by reaction (2), experimentally reproduced from ca. 60 km to subarc depth conditions (Ulmer and Trommsdorff, 1995, 1999; Wunder and Schreyer, 1997). Additional fluid is released by chlorite breakdown, leading to formation of garnet-bearing assemblages (Fumagalli and Poli, 2005; Dvir et al., 2011): no constraints yet exist on the composition of the chlorite-dehydration fluid.

Breakdown of serpentinzed mantle via reaction (2) is recorded in two main localities: Cerro del Almirez (Spain), where chlorite harzburgite crops out as discrete rock unit, and Cima di Gagnone (Central Alps), where chlorite harzburgite and garnet metaperidotite blocks are embedded in a sedimentary mélange. At both localities the serpentinized protoliths are either preserved as relict bodies inside the chlorite harzburgite (Almirez; Trommsdorff et al., 1998), or as serpentine inclusions in peak minerals (Gagnone; Scambelluri et al., 2014). The antigorite breakdown fluids were analyzed only in the Almirez rocks: they correspond to polyphase inclusions hosting olivine, magnetite, a hydrous phase and liquid water enriched in B, Li, alkalis, Pb, Sr (Scambelluri et al., 2001; 2004a, b). Comparable fluid compositions were experimentally achieed by dehydration of natural Almirez serpentine (Spandler et al., 2014). Together, these results show that serpentinite dehydration fluids are viable agents for metasomatism of the subarc mantle.

Exchange with surrounding sedimentary rocks may lead to serpentinite enrichment in specific tracers like As, Be and Sb (Gagnone), in radiogenic Sr and Pb (Gagnone and Almirez) and in light B isotopes (Cannaò et al., 2013; Angiboust et al., 2014). Element addition in serpentinized rocks occurred during prograde burial in Gagnone (Scambelluri et al., 2014; Cannaò et al., 2013), during peak eclogite-facies dehydration in Almirez (Marchesi et al., 2013; Harvey et al, 2014), or during fluid channeling along shear zones within subducting slabs (Angiboust et al., 2014).

Although much work has been done to understand serpentinite behavior in subduction zones, the direct analyses of de-serpentinzation fluids are still few (Scambelluri et al., 2001; 2004 a, b; Tenthorey and Hermann, 2004; Spandler et al., 2014). Here we address this issue by analyzing natural fluid-related inclusions hosted in eclogitic garnet and olivine in the Gagnone metaperidotites. Because these rocks record influx of sediment-equilibrated fluid during prograde subduction metamorphism (Scambelluri et al., 2014; Cannaò et al., 2013),

100 they represent proxies of mantle metaperidotite metasomatized by slab fluids, as occurs in
101 mélange (Bebout, 2007) and/or in supra-subduction zone mantle (Hyndman and Peacock,
102 2003; Savov et al., 2005; Scambelluri et al., 2008). We present textural observations together
103 with fluid inclusion analysis, with the aim to quantify the composition of serpentine-
104 breakdown fluids and constrain element recycling during subduction.
105
106 **2. Geologic and petrologic background**
107 The Cima di Gagnone (Adula-Cima Lunga Unit, Central Swiss Alps) garnet metaperidotite and
108 chlorite harzburgite investigated here originate from lenses inside paragneiss sequences. Like
109 other peridotite bodies (Alpe Arami, Duria) they are exposed along a continuous horizon in
110 the southern Adula Unit (Moeckel, 1969; Fumasoli, 1974; Evans & Trommsdorff, 1978;
111 Pfiffner & Tromsdorff, 1998), associated with pelitic, mafic and granitoid rocks referred to the
112 European continental margin involved in Alpine subduction and collision. The Adula Unit is
113 affected by high-pressure metamorphism (Heinrich, 1982; 1986), that is absent in the other
114 Central Alpine Units and pre-dates widespread collision-related Lepontine amphibolite-facies
115 metamorphism (Trommsdorff, 1966). The Adula rock association has been interpreted as a
116 '*lithospheric mélange*' (Trommsdoff, 1990) formed in a *tectonic accretionary channel* (Engi et
117 al., 2001) representative of plate-interface environments (Engi et al., 2001; Scambelluri et al.,
118 2014).
119 At Gagnone, chlorite harzburgite lenses are the most widespread; garnet metaperidotite
120 is much less frequent. The chlorite harzburgite bodies host eclogite and metarodingite. The
121 latter rocks suggest that the ultramafic host was serpentinized before peak eclogite-facies
122 dehydration (Evans and Tromsdorff, 1978). Petrography, thermobarometry and
123 pseudosection modelling of the Gagnone garnet metaperidotite document a peak eclogite-
124 facies paragenesis of olivine, clino- and orthopyroxene, Mg-hornblende and garnet,

125 crystallized at 800-850 °C and maximum 3 GPa (Fig. 1a; Evans and Trommsdorff, 1978;
126 Pfiffner and Trommsdorff, 1998; Nimis and Trommsdorff, 2001; Fumagalli and Poli, 2005;
127 Scambelluri et al., 2014). In garnet metaperidotite, garnet grows as peak poikilobastic phase
128 that encloses inclusions of prograde chlorite and Ca-amphibole (Fig. 1a; Scambelluri et al.,
129 2014). The peak eclogite-facies paragenesis of chlorite harzburgite consists of olivine,
130 orthopyroxene, chlorite, fluorine-bearing Ti-clinohumite ± carbonate (Trommsdorff and
131 Evans, 1983; Scambelluri et al., 2014). For this rock type, thermodynamic modelling suggest
132 peak crystallization above 650 °C (the antigorite-out reaction) and below 750-800 °C (the
133 chlorite-out reaction; Scambelluri et al., 2014); pressure is likely below 3GPa (Fig. 1b).
134 The major and rare earth element (REE) variability of metaperidotites was mostly
135 acquired during pre-subduction mantle evolution, during partial melting and reactive melt
136 flow in the oceanic plate (Scambelluri et al., 2014). The ultramafic suite is also characterized
137 by fluid-mobile element enrichment. Similarity between the U, Pb, B, Li and Sr concentrations
138 of the Gagnone metaperidotites (Scambelluri et al., 2014) and present-day oceanic
139 serpentinites (Kodolanyi et al., 2012) suggests that these elements were partly uptaken
140 during initial serpentinization by seawater-derived fluids (Scambelluri et al., 2014).
141 Prominent positive Be, As and Sb anomalies suggest involvement of fluids equilibrated with
142 crustal (metasedimentary) reservoirs during prograde subduction metamorphism and
143 metaperidotite entrainment in (meta)sediments (Scambelluri et al., 2014; Fig. 1c). Exchange
144 with sediment-derived fluids is also suggested by metaperidotite enrichment in radiogenic Sr
145 and Pb to values approaching the composition of country metasediments (Cannaò et al.,
146 2013). These specific fluid-mobile element enrichments are detected in all peak eclogitic
147 minerals, and clearly indicate open system prograde subduction metamorphism preceding
148 the eclogite-facies dehydration. The B, Li, As and Sb concentrations of peak anhydrous
149 minerals exceed primitive mantle values, demonstrating the potential of dehydrated

150 serpentinite residues to transfer geochemical anomalies deep into the Earth's mantle.

151

152 **3. Inclusion occurrence and petrography**

153 The inclusions inside the high-pressure minerals of the Gagnone metaperidotites can be
154 grouped as: (1) monophase mineral inclusions; (2) polyphase inclusions, hosting a number of
155 minerals intergrown in regular cavities.

156 The first group represents remnants of the pre-eclogitic mineral parageneses and occurs
157 in all metaperidotites. In garnet metaperidotite, prograde chlorite, amphibole, ortho and
158 clinopyroxene inclusions are overgrown by eclogitic poikiloblastic garnet. This indicates that
159 these rocks, besides antigorite dehydration, record later-stage chlorite breakdown and garnet
160 formation (Fig. 1a). In chlorite harzburgite, inclusions of prograde serpentine are preserved in
161 eclogitic fluorine-Ti-clinohumite. The reader is referred to Scambelluri et al. (2014) for more
162 detailed descriptions and for discussion of implications.

163 Microscopy in reflected light has revealed several opaque phases, corresponding to light-
164 grey chromite, magnetite and yellowish sulfides. The latter occur as single inclusions in
165 minerals, as rims and/or overgrowths on chromite, and as interstitial crystals in-between
166 high-pressure minerals; they frequently consist of intergrown crystals of variable chemical
167 composition. Rock-forming sulfides are more abundant in chlorite harzburgite than in garnet
168 metaperidotite.

169 Polyphase inclusions occurs in garnet and olivine from garnet metaperidotite, and in
170 olivine and orthopyroxene from chlorite harzburgite.

171 *Garnet metaperidotite* contains coarse garnet layers and shows coarse centimetres-sized
172 garnet crystals that may correspond to veins or fluid pockets (Figs. 2a, 2b). The coarse garnet
173 (sample MG160-C1) contains myriads of solid polyphase inclusions whose shapes range from
174 geometrically regular to irregular cavities. In general, they are randomly dispersed in garnet

(Figs. 2c,d,f) and are thus interpreted to represent primary fluid inclusions. Similar polyphase inclusions in garnet also occur along planes that do not intersect the garnet grain-boundaries (Fig. 2e). Therefore these inclusions are interpreted to be pseudosecondary. The polyphase inclusions in olivine close to garnet (MG160-C1) are comparable: they are randomly distributed inside olivine and also aligned along microcracks which do not crosscut the olivine grain-boundaries, like primary and pseudosecondary inclusions, respectively (Fig. 4). The inclusions display opaque phases and transparent, birefringent crystals. The polyphase inclusions exposed at the mineral surface contain solids and yellowish sulfide microcrystals. Scanning electron microscopy of exposed, olivine-hosted inclusions has revealed that between inclusion and olivine host a reaction halo made of new olivine developed during post-entrapment fluid-olivine reaction still in the olivine stability field (Fig. 3a). Olivine microcrystals were also identified inside the inclusions (Fig. 3b).

In *chlorite harzburgite,* the polyphase inclusions are hosted by olivine, less frequently by orthopyroxene, and occur only in coarse undeformed samples (MG304-92-1, MG304-92-2). In such samples, rock-forming magnesite can be part of the high-pressure assemblage (Fig. 3c; MG304-92-2) and is partly replaced by rims of retrograde dolomite. The chlorite harzburgite also shows tiny sulfide grains, occurring as inclusions in rock-forming minerals and as interstitial phases in-between high-pressure minerals (Fig. 3d). As for the garnet metaperidotite, the polyphase inclusions are regular to irregular in shape, are mostly randomly dispersed in the host minerals, range in size from several micrometers (the majority) to several tens of micrometers, and contain opaque crystals together with transparent, birefringent phases (Fig. 3e); they rarely follow pseudosecondary trails. Scanning electron microscopy shows the occurrence of olivine (Fig. 3b) and of sulfide microcrystals inside inclusions.

200 **4. Fluid inclusion data reduction**

201 Major element concentrations in inclusion-forming minerals, elemental maps of inclusions,
202 scanning electron microscopy of inclusions, and analysis of the trace element composition of
203 inclusions and hosts were performed by electron microrobe, scanning electron microscopy
204 and laser-ablation-ICP-MS in the Universities of Milano, Genova and Bern. Analytical mehods
205 are described in the repository files.

206 Data reduction for polyphase inclusion analysis followed the principles developed in Halter et
207 al. (2002). Because an element concentration in the polyphase inclusions cannot
208 independently be determined but is required as the internal standard for data reduction, we
209 adopted the procedures described in detail below. The entire data set is provided in electronic
210 Repository Table R4; inclusion data with consistent patterns are presented here in Table 1.
211 (1) For garnet-hosted fluid inclusions (sample MG160-C1): Iron shows compatible behavior in
212 the garnet - aqueous fluid system at 4 GPa/800 °C for basaltic bulk composition ($KD_{Fe(fluid\text{-}grt)}$ =
213 0.016; Kessel et al., 2005). Because element distribution coefficients tend to decrease with
214 increasing pressure in aqueous fluid mineral pairs, we employed a $KD_{Fe(fluid\text{-}grt)}$ = 0.01 to
215 derive the concentration of FeO = 1.07wt% for the fluid inclusions from the measured garnet
216 FeO = 10.7wt%. We further assumed a total dissolved load of 20wt% for the inclusion fluids,
217 estimated again on the basis of data at 4 GPa/800 °C (Kessel et al., 2005). With this approach,
218 3 out of 6 high-quality inclusion analyses returned a constant SiO_2 concentration of ca.
219 10wt%. This SiO_2 concentration was then employed to calculate the element concentrations
220 of the other 3 inclusions, which returned an FeO concentration of ~2.1wt% instead of the
221 inferred 0.17wt%. Note that Fe was calculated exclusively as FeO, lacking constraints on the
222 oxidation state of Fe in the fluid at entrapment. These data suggest that two different types of
223 fluid inclusions were trapped in garnet.

224 (2) Olivine-hosted inclusions were analyzed for two samples.

225 (2a) For garnet metaperidotite sample MG160-C1, assuming a low Na_2O concentration as
226 above for data reduction did not return results except for two analyses (21frc04; 21frc10). Of
227 these, analysis 21frc04 returned a Na_2O/TiO_2 ratio of 0.08 along with elevated FeO,
228 suggesting accidental entrapment of a Ti-rich mineral (ilmenite?). Therefore, assumed Na2O
229 concentrations of the fluid were incrementally increased for calculation. For Na_2O = 0.5wt%
230 results were obtained for 6 inclusion analyses (21frc06, 21frc08, 21frc09, 21frc11, 21frc12,
231 21frc13). Interestingly, 5 of these show consistent molar Na/Cl ratios of between 0.33 and
232 0.46. Of these, all but inclusion 21frc08 (FeO below detection) returned an FeO concentration
233 of between 1.0 and 1.6wt%. Other two inclusions returned results for an assumed Na_2O =
234 0.1wt%. While their major element pattern is consistent with the inclusions above, their
235 molar Na/Cl ratios are 0.9 and 1.3, respectively and thus clearly different. We therefore use
236 inclusions 21frc09, 21frc11, 21frc12, 21frc13 for further evaluation.
237 (2b) For chlorite harzburgite sample MG304-92-2, a concentration of 0.01wt% Na_2O and
238 10wt% of total dissolved solids was assumed, based on the Na_2O concentration obtained for
239 the garnet-hosted inclusion and the fact that primary inclusions in olivine were likely
240 entrapped at lower P-T than those in garnet (and thus the total dissolved solids are assumed
241 to be lower as argued above). With these constraints, inclusion concentrations could not be
242 calculated for 7 out of 16 inclusions, indicating that they represent mixtures of fluid inclusions
243 and accidentally trapped Cr and Al-bearing Fe-rich spinel. Of the remaining inclusions, that
244 returning an MgO concentration below its limit of detection (analysis 21fra04) and those with
245 an Al_2O3 > 1.5wt% and Cr > 1400µg/g (analyses 21fra12 and 21fra17) were discarded as
246 outliers. Finally, 6 inclusion analyses remained with consistent inclusion element
247 concentrations.
248
249 **5. Mineral content and major element composition of inclusions**

250 Electron microscopy, elemental maps of inclusions, and microprobe analysis of inclusion-
251 forming minerals enabled to identify the main mineral species inside the inclusions. Analyses
252 are reported in Repository Tables R1, R2, R3; the maps of garnet- and of olivine-hosted
253 inclusions are shown in Figures 4 and 5, respectively.

254 *Garnet Metaperidotite.* The maps showing element distribution inside polyphase
255 inclusions in garnet (Fig. 4) reveal the presence of Cl as inclusion component. Chlorine is
256 absent, or below detection in the garnet host. Coincidence in the distribution of Cl, K and Fe
257 suggests the presence of chloride phases. Chlorine is not ubiquitous in garnet-hosted
258 inclusions, because some of them do not reveal detectable amounts of this element (both by
259 SEM and LA-ICP-MS data). Figure 4 also shows the presence of Cr-bearing oxides and of Cu-
260 (and As) bearing sulfides, consistent with the LA-ICP-MS data. In all analyzed inclusions the
261 remaing phases correspond to Ca-amphibole, chlorite and spinel (see Tab. R1). Presence of
262 such mineral infillings in garnet-hosted inclusions is again confirmed by the high Ca and Cr
263 concentrations shown by bulk inclusion analyses (Tab. 1). In some cases, electron microscopy
264 points out that some inclusion minerals can derive from reaction with the host mineral. Ca-
265 amphibole + spinel intergrowths in garnet immediately surrounding the polyphase inclusions
266 can derive from reaction between fluid and host garnet after inclusion entrapment, or may
267 represent the preferred formation of fluid inclusions along with accidentally trapped spinel
268 crystals. While the former poses no limitations to the bulk fluid composition, the latter
269 produces mixtures whose composition is meaningless and therefore discarded from the
270 dataset (analysis 21frc04).

271 Comparable textures affect the olivine-hosted inclusions in garnet metaperidotite (Fig. 5).
272 Olivine from sample MG160-C1 contains inclusions filled with Cr-bearing Fe-oxide, magnetite,
273 Cl-bearing phase and Ni sulfide. The latter differs from sulfide from garnet-hosted inclusions
274 because it lacks Cu and Ni is present as major component (Tab. R3). As a whole, analyses of

275 the olivine-hosted inclusions yield much more Ni than the garnet-hosted inclusions (Tab. 1),
276 which might be either due to post-entrapment diffusional equilibration between inclusion and
277 host, or to incomplete removal of host olivine during LA-ICP-MS data reduction. Indeed, the
278 inclusions in olivine from garnet metaperidotite and chlorite harzburgite display reaction
279 haloes in the host made of magnesian silicates (olivine and/or serpentine) against the host
280 (Fig. 3a), pointing to post-entrapment interaction between fluid and olivine host.

281 *Chlorite harzburgite*. Inclusions were investigated in carbonate-free (Mg304-92-1) and
282 carbonate-bearing chlorite harzburgite (Mg304-92-2), where magnesite and dolomite are
283 peak and retrograde rock-forming minerals, respectively. Inclusions in olivine of the
284 carbonate-free sample contain Fe-oxide, Cl-bearing phase and Ni sulfide (Fig. 5). The opaque
285 minerals differ from those of inclusions in garnet for lower Cr content of oxide and for
286 presence of Ni as main sulfide component (Tab. R3). Same as the garnet-hosed inclusions, the
287 above opaque phases are associated with chlorite and serpentine. The latter locally appears to
288 overgrow former olivine, showing a different electronic image but whose analysis was
289 hampered by the small olivine size (Fig. 3b).

290 In the carbonate-bearing sample MG304-92-2 magnesite occurs as rock-forming mineral
291 coexisting with high-pressure olivine, orthopyroxene and chlorite (Scambelluri et al., 2014,
292 their Fig. 3a). It is overgrown by rims of retrograde dolomite. In this sample, magnesite also
293 occurs as inclusion-forming mineral together with serpentine, chlorite, magnetite. Magnesite
294 precipitation in inclusions indicates the presence of carbon species in the dehydration fluid
295 within this sample. Interestingly, the inclusion magnesite also shows partial replacement by
296 dolomite. This finding, together with evidence of inclusion-olivine replacement by serpentine,
297 suggests precipitation of high-pressure phases within fluid-inclusions, followed by their
298 replacement during back reaction with the inclusion fluid during retrograde metamorphism
299 and exhumation.

6. Trace element compositions of inclusions

LA-ICP-MS analyses of inclusions in garnet metaperidotite and chlorite harzburgite are reported in Tables 1 and R4. The time-resolved analyses (Fig. 6) of inclusions hosted by garnet (Fig. 6a) and olivine (Figs. 6b; c; d) reveal detectable peaks in fluid-mobile elements and LILE. The inclusion compositions are portrayed in Figure 7 as spidergrams normalized to Primitive Mantle (PM, McDonough and Sun, 1995).

In garnet metaperidotite, the olivine-hosted inclusions display strongly elevated concentrations of Cs, Rb, Ba, Pb, As, Sb, Sr and Cl (up to 1000 PM) and moderate enrichments of B, U and partly Li (up to 10 PM; Fig. 7a). Because only a few of all trace elements returned significant concentrations for the host olivine (due to the smaller beam size employed for inclusion analysis and to the fact that detection limits negatively correlate with beam size), measured element distribution coefficients obtained from these analyses are limited. $KD_{(fluid/olivine)}$ for inclusion-host olivine pairs range considerably; hence, only orders of magnitude can be estimated (Si, Mg, Fe $\sim 10^1$, As $\sim 10^2$; Na, Sr, Pb $\sim 10^3$); however, Ti = 0.5 and Li = 4 are well constrained. An alternative approach is to estimate $KD_{(fluid/olivine)}$ values by combining the fluid data with large-beam (and thus low LOD) analyses of olivine from the same rock sample (published in Scambelluri et al., 2014). This approach returns $KD_{(fluid/olivine)}$ = 4 for Li (identical to that above), for B = 3 (consistent with Scambelluri et al., 2004a; Tenthorey and Hermann, 2004), for As = 350, for Sr = 33000, and for Sb = 1230. Even with large beam sizes, olivine analyses did not return significant concentrations for several elements. In such cases, miminum $KD_{(fluid/olivine)}$ values can be estimated based on the element-specific lower LOD values obtained (plotted in Fig. 8a with a vertical arrow pointing downwards). This way we obtain for Rb = 3500, for Cs = 10000, for Ba = 25000, for Y = 80, for La = 830, for Ce = 650, for Nd = 40, for Dy = 20, for Pb = 8300 and for U = 90. This strongly

suggests extreme LREE enrichments in fluids coexisting with olivine, very similar to fluid patterns observed in the water-basalt system at 4-6 GPa (Kessel et al., 2005b).

The garnet-hosted inclusions of this sample are different (Fig. 7b). The LILE and fluid-mobile element enrichments are less pronounced than for the olivine-hosted inclusions. Cesium, Rb, B, As, Sb and Li show PM-normalized values above 1 while most other elements are below 1. Significant measurements for elements in garnet were only obtained for MREE to HREE, Li, and Nb. The few, directly determined element distribution coefficients show $K_{D(fluid/garnet)}$ values between ca. 0.2 and 0.05 for the REE (decreasing with increasing atomic number), and in the order of 10 for Li. $K_{D(fluid/garnet)}$ values for Sr and Nb are around 4 and 1.7, respectively. For the other elements, it is not useful to report minimum $K_{D(fluid/garnet)}$ values, because the respective detection limits for these elements are at the lower end of the ranges covered by the fluid element concentrations (compare with Tab. R4).

The olivine-hosted inclusions in chlorite harzburgite (MG204-92-2) are different from the olivine-hosted inclusions in MG160-C1 and resemble those hosted by garnet in this sample (Fig. 7c; Tab. 1). Concentrations relative to PM are again most enriched for As and Sb, followed by Cs and B. Lead shows PM concentrations, and the other elements are variably below PM values. As for garnet in MG160-C1, only a few of the host olivine element concentrations are significant; most elements were below the respective LOD's. Estimated $K_{D(fluid/olivine)}$ for As is about 100, while for B, Nb, Ta, Zr it is around 1 and for Li it is ~0.2.

Alltogether, prominent enrichments in As and Sb and variably enriched large ion lithophile elements plus positive PM-normalized anomalies for B and partly Pb characterize all inclusion compositions, while Sr is only enriched in the olivine-hosted inclusions of sample MG160-C1. These olivine-hosted inclusions contain a prominent halogenide component (~1.5wt% Cl) that is absent from inclusions hosted by garnet or in olivine from the chlorite harzburgite (Tab. 1), thus demonstrating that two different fluid inclusion generations are

present in these samples. The least prominent relative LILE enrichment is revealed by olivine-hosted inclusions of chlorite harzburgite MG304-92-2, consistent with the corresponding low bulk rock values (Scambelluri et al., 2014) of 0.014µg/g Cs, 0.052µg/g Rb, 0.83µg/g Ba and the depleted LREE concentrations (e.g., 0.085µg/g La) indicative of prominent melt depletion prior to hydration.

7. Discussion

The garnet metaperidotite and chlorite harzburgite from Cima di Gagnone are the high-pressure breakdown products of mantle rocks affected by multiple serpentinization stages, oceanic and subduction-related (Evans and Trommsdorff, 1978; Scambelluri et al., 2014). Positive anomalies in As, Sb, Be, elevated contents in radiogenic Sr, Pb and low $\delta^{11}B$ characterizing bulk rocks and high-pressure minerals point to exchange between the serpentinzed peridotite precursors and the enclosing paragneiss during subduction burial (Scambelluri et al., 2014; Cannaò et al., 2013). This geochemical record candidates Gagnone as prime example of metaperidotitic slab lenses in subduction mélanges, or of slices of hydrated supra-subduction zone mantle entrained into the subduction plate interface. In Gagnone, the prograde dehydration evolution presented in the pressure-temperature diagrams of Figure 1 is indicated by relict (metastable) serpentine and chlorite + amphibole inclusions in eclogite-facies minerals of chlorite harzburgite and garnet metaperidotite, respectively. This indicates that chlorite harzburgite and garnet peridotite underwent antigorite breakdown that, in garnet peridotite, was followed by chlorite dehydration (Fig. 1a, b).

7.1. Inclusion textures and post-entrapment modifications

The garnet- and olivine-hosted polyphase inclusions presented here further constrain the dehydration process that affected the metaperidotite protoliths. In terms of texture, the

polyphase inclusions are comparable with primary and pseudosecondary fluid inclusions, i.e., randomly dispersed in the core of high-pressure minerals or as inclusion trails that do not intersect grain boundaries (Fig. 2e). Despite deriving from devolatilization reactions releasing water-rich fluids, the Gagnone inclusions do not correspond to liquid-rich aqueous fluids, but are filled with minerals. This indicates post-entrapment modifications that need to be addressed first.

Post-entrapment modifications can be isochemical and non-isochemical, and the latter need to be recognized in order to understand the significance of data. Post-entrapment crystallization in response to H or water loss does not pose analytical problems as long as the entire inclusion content is analyzed, as for example via drilling out complete inclusions from host minerals by LA-ICP-MS. Laboratory re-homogenization of inclusion contents (via reheating) is not viable because of H or water loss. Strictly, solvent loss qualifies the process of post-entrapment crystallization of eclogite-facies fluid inclusions as non-isochemical; however, the total dissolved solids load may remain unchanged. Non-isochemical post-entrapment modifications include diffusive equilibration with the host mineral or possibly with the surrounding rock materials and are indicated by magnetite crystallization in the inclusions. The model reaction fayalite (in olivine)+$H_2O \rightarrow SiO_{2(aq)}$ + magnetite + H^+, followed by H-loss, documents gain of Fe and increased f_{O2} in the fluid inclusion upon crystallization.

Evidence that mineral precipitation in inclusions began under elevated temperature (and high-pressure) conditions is provided by crystallization of olivine onto the inclusion walls, by olivine micro-crystals in inclusions (Fig. 3a,b), and by presence of magnesite in inclusions from magnesite-bearing chlorite harzburgite. The inclusion magnesite likely has lower Mg and higher Fe than the rock forming magnesite, though the small size of carbonate inside inclusions prevented satisfactory analytical work. Amphibole + spinel reaction rims associated with Cu-bearing sulfide occur in garnet-hosted inclusions, while the olivine-hosted

inclusions of the same sample and of MG304-92-2 contain Mg-silicates and Fe-Ni sulfides without significant Cu (Figs. 4; 5). These Ni-bearing sulfides in the olivine-hosted inclusions may be a reaction product with the olivine host. The differences in inclusion mineralogy may therefore indicate post-entrapment interaction between inclusions and their host. These interactions certainly affected major element fluid inclusion composition. However, incompatible trace element patterns likely remain unaffected, in very much the same way as for silicate melt inclusion (e.g., Danyushevsky et al., 2000; Pettke, 2006; Audetat and Lowenstern, 2014) and as suggested by previous work on high-pressure polyphase inclusions (e.g. Scambelluri et al., 2004a; Malaspina et al., 2006). Therefore, such high-pressure polyphase inclusions can preserve important compositional information on the nature of high-pressure fluids and document major fluid-processes during the subduction cycle.

The similarity to polyphase inclusions from the Almirez chlorite harzburgite is striking. Both inclusion types contain chlorite, olivine (or serpentine), opaque minerals plus additional minor phases (apatite in Almirez, chlorides in Gagnone; see Scambelluri et al., 2001). Scambelluri et al. (2001; 2004a) estimate that the water-rich antigorite breakdown Almirez fluid inclusions (with salinity between 0.4 and 2wt% NaCl) were desiccated by precipitation of hydrous silicates and H^+ loss during during post-entrapment fluid inclusion modification.

7.2 Fluid inclusion compositions

Concerning fluid components, the elemental maps of Figures 4 and 5 and sulfide analysis (Fig. 8) complement the inclusion compositional data and help identifying the elements transported by the fluid. Elemental mapping sometimes revealed the presence of Cl, often along with K and Fe. Chlorine anomalies only pertain to polyphase inclusions and are absent in other rock domains. For this reason we propose that Cl was a high-pressure fluid component, as pointed out by the significant Cl concentrations measured in olivine-hosted

425 inclusions from garnet peridotite MG160-C1 (Tab. 1). Serpentinite dehydration is known to
426 release chlorine-bearing fluids, especially during antigorite + brucite → olivine + H_2O reaction
427 (Scambelluri et al., 1997; 2004; Kodolanyi and Pettke, 2011). Scambelluri et al. (2004)
428 estimated a bulk loss of 2wt% H2O during this reaction. Chlorine concentrations in antigorite
429 dehydration fluids are lower (0.4-2wt% NaCl in fluid; Scambelluri et al., 2004a) because the
430 larger amount of water produced by the antigorite breakdown reaction (5 to 10wt% H_2O)
431 strongly dilutes the fluid. Presence of chlorine in the Gagnone polyphase inclusions therefore
432 confirms that dehydration of serpentinized ultramafic rocks releases Cl to fluids. The analysis
433 of sulfide at different textural sites of garnet peridotite and chlorite harzburgite points to a
434 change in sulfide composition during rock evolution, probably depending on fluid
435 composition. Figure 8 shows variation in sulfide composition from higher S and Fe
436 concentrations measured in rock-forming grains (mineral inclusions and interstitial
437 minerals), to lower Fe and S and higher Ni and/or Cu in sulfide crystals inside inclusions. In
438 the Gagnone metaperidotites, formation of sulfide phases that are not stable in pristine
439 mantle rocks and in altered seafloor mantle indicates sulfur mobility during subduction
440 metamorphism and suggests presence of reduced sulfur in the high-pressure fluids.
441 The presence of magnesite in inclusions from chlorite harzburgite provides compelling
442 evidence that, besides water, carbon is also a key component of the metaperidotite
443 dehydration fluid. Either decarbonation or magnesite dissolution was responsible for carbon
444 release into the aqueous deserpentization fluid. The available data do not constrain the C:O:H
445 abundance ratios of the fluid at entrapment conditions, however.
446
447 *7.2.1. Trace element inclusion compositions*
448 The trace element patterns of the fluid inclusion presented here suggest the presence of two
449 types of fluids in these rocks, one trapped in olivine of garnet peridotite MG160-C1 and one

450 trapped in garnet of this sample and in olivine of chlorite harzburgite MG304-92-2 (Fig. 7).
451 Olivine-hosted inclusions in MG160-C1 (type A; Fig. 7a) are quite enriched in fluid-mobile
452 elements (Cl, Pb, As, Sb, Tl, Cs, Rb, Ba; to a lesser extent B, Li and U) relative to primitive
453 mantle and to the type B fluid trapped in coarse garnet from the same sample (MG160-C1; Fig.
454 7b) and in olivine from chlorite harzburgite MG304-92-2 (Figure 7c; Tab. 1). However, the
455 PM-normalized patterns for the two fluid types are very similar (Fig. 9a) and show As, Sb,
456 ±Pb, ±Cs, ±Li above 1, but the latter fluid type appears much less enriched in fluid-mobile
457 elements. Type A fluid has up to 10^3 PM for Cl, Cs, Pb, As, Sb and ~10^2 PM for Tl, while Rb, Ba,
458 B, Sr are ~10^1 PM, and Na, K are ~2 PM. The combined enrichment of LILE and chalcophile
459 elements coincides with what is expected to be characteristic for a sediment-equilibrated
460 fluid. Type A fluid thus records a much more prominent sediment signal than does type B
461 fluid, a difference that can be related to multiple dehydration stages of rocks recording
462 different extents of pre-eclogitic interaction with sediment-derived fluids. In garnet
463 peridotite, fluid A and B in olivine- and in garnet-hosted inclusions, respectively, can be
464 related to different fluid-forming dehydration reactions and stages. Since the poikiloblastic
465 (rock-forming) and the vein-type garnet (Fig. 2a, b) crystallized late in these rocks, the garnet-
466 hosted inclusions can trap the fluid evolved during chlorite breakdown to garnet. Differently,
467 the olivine-hosted inclusions in the garnet metaperidotite may derive from earlier-stage,
468 antigorite dehydration (Fig. 1). In this perspective all olivine-hosted inclusions in garnet
469 metaperidotite (Fig. 9a) and in chlorite harzburgite (Fig. 9c) can derive from antigorite
470 breakdown: the different fluid-mobile elements concentrations of such inclusions (Figs. 7; 9)
471 can be related to variable intensities of precursor rock interaction with sediment-derived
472 fluids prior to eclogitic peak.

473 In summary, our analytical survey indicates that the chlorite harzburgite and the garnet
474 peridotite lenses from Gagnone trap fluids related to multiple dehydration stages recorded by

475 rocks affected by different degrees of interaction with sediment-derived fluid prior to
476 eclogitization.
477
478 *7.4. Relevance for trace element cycling in the subduction interface*
479 Presence of the same set of elements in the fluid-related inclusions and in high-
480 pressure minerals grown during metaperidotite dehydration implies a recycling process and
481 candidates the Gagnone metaperidotites as useful materials (i) for tracing fluid-mediated
482 trace element crust-mantle exchange, and (ii) for understanding the composition of
483 subduction fluids released by such a metasomatized mantle reservoir. The P-T conditions
484 metaperidotite recrystallization (800-850 °C; 3 GPa) fit recent modelling of top slab
485 temperatures in sub-arc subduction domains (Syracuse et al., 2010). The Gagnone fluid-
486 related inclusions are compared in Figure 10b with primary inclusions in chlorite harzburgite
487 from Cerro del Almirez (Scambelluri et al., 2004b). At both localities the inclusions display
488 comparable PM-normalized trace element patterns, showing positive spikes in fluid-mobile
489 Cs, Rb, Ba, B, Pb, Li (Fig. 9b; As and Sb data are not available for Almirez). From this
490 comparison it emerges that the de-serpentinization fluids in the two localities display
491 common features, represented by Cs, B, Pb and Li concentrations exceeding those of primitive
492 mantle. The PM-normalized pattern of the Gagnone fluid inclusions also compares well with
493 compositions of an antigorite breakdown fluid trapped in fluid inclusion during experimental
494 dehydration of natural serpentinite from Almirez (Fig. 9c) by Spandler et al. (2013). We thus
495 interpret these fluid data to represent a common serpentinite subduction fluid signature,
496 while prominent positive anomalies of As, Sb, Tl, Rb, Cs and Ba to this elemental budget
497 indicate input of a crustal (sedimentary) component to the de-serpentinization fluid.
498 Figure 7 shows that inclusions and host high-pressure minerals can have quite
499 different absolute trace element concentrations and patterns. This is the case for Cs, Rb, Ba, U

and Pb in olivine-hosted inclusions, showing high concentrations in such elements (up to hundreds times the PM in olivine-hosted inclusions from garnet metaperidotite) that are virtually absent in the mineral host. In such inclusions As, Sb and Tl are quite abundant. The same reasoning can be applied to Cs, B, As and Li in garnet-hosted inclusions. This different behaviour encourages the use of mineral/fluid partition coefficients (Fig. 9d), calculated for several elements using the average compositions of polyphase inclusions (Table 1) and of mineral hosts (see section 6). As expected, garnet has affinity for Zr, Y, HREE whereas olivine can retain significant Li and B, as shown by $KD_{(fluid/olivine)}$ close to 3 and 4, as also documented in previous studies (Tenthorey and Hermann, 2004; Scambelluri et al., 2004a). This fact was already underlined for the Almirez chlorite harzburgite, hosting unexpectedly high amounts of fluid-mobile elements, even noble gases, expected to preferentially leave the solid phases during dehydration processes (Scambelluri et al., 2001, 2004a: John et al., 2011; Kendrick et al., 2011). Therefore, the dehydrated, high-pressure metaperidotite residues can introduce fluid-mobile element anomalies in the convecting mantle.

Arsenic, Sb, Be and part of the whole-rock Pb, B, Sr of the Gagnone metaperidotite were acquired via exchange with metasedimentary country rocks during subduction burial (Scambelluri et al., 2014; Cannaò et al., 2013). The capacity of serpentinized mantle to incorporate fluid-mobile elements was emphasized by Hattori and Guillot (2003) and by Deschamps et al. (2011), showing that As, Sb, B lost from dehydrating slabs at relatively low-temperature are transferred to altered ultramafic (mantle) lithologies. The high concentrations of such fluid-mobile elements measured in the Gagnone bulk rocks, fluid-related inclusions and high-pressure minerals fits the above interpretation, and points out that As, Sb, Cs, Rb, Tl (together with radiogenic Pb and Sr; Cannaò et al., 2013) were *'fluid-transported'* from the country paraschist into the mélanged ultramafic bodies. The compositions of the hydrated Gagnone metaperidotite protoliths are reconstructed in Figure

525 9e using the mineral/fluid partition coefficients of Figure 9d, together with the modal
526 amounts of rock-forming olivine and garnet in garnet metaperidotite (amphibole, ortho and
527 clinopyroxene have been omitted from this estimate due to a lack of coupled fluid inclusion
528 and host measurements). Figure 9e shows that the trace element patterns of abyssal, mantle
529 wedge and subduction-zone serpentinites (Deschamps et al., 2013) and of the Gagnone garnet
530 metaperidotite protoliths are comparable, the main difference being much higher absolute
531 concentrations of Cs, Rb, Ba, La, CePb, As, Sb, Sr, Nd of the Gagnone rocks prior to dehydration.
532 Because of the magnitude of these differences, the Cima di Gagnone garnet metaperidotite
533 pattern emphasizes the crustal (sedimentary) input recorded by these rocks. Therefore, they
534 may represent an ultramafic end-member for uptake of crust-derived elements.

535 The local-scale trace element transfer documented here for Gagnone may have larger-
536 scale implications when considering slab to supra-subduction zone mantle transfer of fluids
537 and elements. A possible interpretation arising from Figure 9b is that Almirez, like Gagnone,
538 underwent fluid-mediated element exchange with associated crustal rocks prior to antigorite
539 breakdown. Crustal gneisses crop out quite close to the Almirez ultramafic body: input from
540 external (sedimentary) reservoirs into serpentinites has been recently advocated by Marchesi
541 et al. (2013) and Harvey et al. (2014) based on trace element and Sr isotopic studies. This may
542 better explain the enrichment in crust-derived elements unusual in serpentinites formed by
543 single-stage ocean floor hydration, and increasingly found in ultramafic rocks evolved
544 through subduction zone processes. If one extrapolates from the context of top-slab mélange
545 environment, and considers the pre-dehydration Gagnone compositions (Fig. 9e) as
546 representative of altered supra-subduction mantle wedge, the potential of ultramafic rock
547 systems in storing and transporting slab-derived elements from shallow (forearc) to deep
548 subduction settings becomes compellingly apparent. As stated previously (Hyndman and
549 Peacock, 2003; Savov et al., 2005; Hattori and Guillot, 2003; Scambelluri and Tonarini, 2012)

550 the shallow-level water transfer from slab to overlying mantle coincides with fluid-mobile
551 element transport. Cannaò et al. (2013) show that this transfer also regards radiogenic Sr and
552 Pb isotopes. Gagnone may therefore represent a highly enriched end-member of this process.
553
554 **8. Conclusions**
555 The Gagnone metaperidotite suite presented here derives from precursor mantle rocks
556 recording: (i) early element uptake during oceanic hydration followed by exchange with
557 sediment-derived fluids during subduction burial; (ii) eclogite-facies dehydration
558 (Scambelluri et al., 2014). The investigated chlorite harzburgite essentially records high-
559 pressure breakdown of serpentine, whereas the associated garnet metaperidotite records a
560 first event of de-serpentinzation followed by chlorite breakdown to garnet.
561 The eclogite-facies olivine and garnet trap primary to pseudosecondary inclusions
562 representing the fluid evolved during breakdown of antigorite (fluid A) and chlorite (fluid B).
563 The inclusions contain fluid-mobile elements (high Cl, S; variable Cs, Rb, Ba, B, Pb, As, Sb).
564 Presence of magnesite in inclusions from metaperidotite samples showing rock-forming
565 eclogitic magnesite indicates carbon release to the aqueous fluid via decarbonation and/or
566 dissolution.
567 The olivine-hosted inclusions in the garnet metaperidotite (fluid A) have the highest fluid-
568 mobile element content and LREE, reflecting a sedimentary signal and the recycling
569 sedimentary components into the de-serpentinization fluid. Lower degrees of enrichments of
570 these elements in olivine-hosted inclusions from chlorite harzburgite point to variable
571 degrees of pre-eclogitic alteration of the Gagnone rocks.
572 The inclusions trapped in garnet (fluid B, deriving from chlorite dehydration) display
573 relatively low fluid-mobile elements, suggesting squeezing of a rock that already delivered
574 such components during serpentine breakdown.

575 Our observations indicate that altered supra-subduction mantle sequesters water, carbon
576 and fluid-mobile elements sourced by slabs, and that dehydration of such a metasomatized
577 mantle provides fluid-mobile element-enriched fluids (like the Gagnone inclusions) to arcs.
578 We confirm the tendency of serpentinized mantle to capture fluid-mobile elements and
579 propose that through fluid-mediated transfer from sediments combined with subduction-
580 zone processing, serpentinzed mantle acts as carrier of specific elements to arcs.
581 The shallow element release from slabs to mantle, its downward flow and its subsequent
582 (subarc) dehydration tranfers the goods to subarc mantle (Hyndman and Peacock, 2003;
583 Ruepke et al., 2004; Savov et al., 2004; Scambelluri and Tonarini, 2012) without need of
584 concomitant subarc dehydration/melting of metasedimentary slab components. Therefore,
585 we conclude that the Gagnone inclusions can represent what is sourced by slab-contaminated
586 mantle peridotite in deep subduction settings.
587

588 **Acknowledgements**
589 The Italian MIUR (PRIN-COFIN 2012; Project 2012R33ECR_002) and the Swiss NSF are
590 aclnowledged for funding.
591

592 **References**

593

594 Alt J.C, Schwarzenbach E.M., Früh-Green G.L., Shanks W.C.III, Bernasconi S.M., Garrido C.J., Crispini L.,
595 Gaggero L., Padrón-Navarta J.A., Marchesi C. (2013) The role of serpentinites in cycling of carbon and
596 sulfur: Seafloor serpentinization and subduction metamorphism. Lithos 178, 40-54a

597

598 Angiboust S., Pettke T., De Hoog C.J.M., Caron B., Onken O. (2014) Channelized fluid flow and eclogite-
599 facies metasomatism along the subduction shear zone. Journal of Petrology 55, 883-916.

600

601 Audetat, A, Lowenstern, J. B. (2014) Melt inclusions. Treatise on Geochemistry, Second Edition, (2014),
602 vol. 13, pp. 143-173.

603

604 Bebout, G.E. (2007). Metamorphic chemical geodynamics of subduction zones. *Earth and Planetary*
605 *Science Letters* **260**, 373–393

606

607 Blanco-Quintero, I.F., García-Casco, A., Gerya T.V. (2011) Tectonic blocks in serpentinite mélange
608 (eastern Cuba) reveal large-scale convective flow of the subduction channel. *Geology* 39, 79-
609 82doi:10.1130/G31494.

610

611 Boschi C., Bonatti E., Ligi M., Brunelli D., Cipriani A., Dallai L., D'Orazio M., Früh-Green G.L., Tonarini S.,
612 Barnes J.D., Bedini R.M. (2013) Serpentinization of mantle peridotites along an uplifted lithospheric
613 section, Mid Atlantic Ridge at 11° N. Lithos 178, 3-23.

614

615 Bostock, M.G., Hyndman, R.D., Rondenay, S. & Peacock, S.M. (2002). An inverted continental Moho and
616 serpentinization of the forearc mantle. *Nature* **417**, 536-538.

617

618 Cannaò, E., Scambelluri, M., Agostini, S., Tonarini, S. (2014) The geochemical fingerprint of

619 serpentinite- and crust-dominated plate-interface settings: some tectonic implications. Geophysical
620 Research Abstracts Vol. 16, EGU2014- EGU General Assembly 2014
621
622 Cannat, M., Mével, C., Maia, M., Deplus, C., Durand, C., Gente, P., Agrinier, P., Belarouchi, A., Dubuisson,
623 G., Humler, E. & Reynolds, J. (1995). Thin crust, ultramafic exposures, and rugged faulting patterns at
624 the Mid-Atlantic Ridge (22°–24°N). *Geology* **23**, 49–52.
625
626 Danyushevsky, L.V., Della-Pasqua, F.N. & Sokolov, S. (2000): Re-equilibration of melt inclusions
627 trapped by magnesian olivine phenocrysts from subduction-related magmas: petrological
628 implications. Contrib. Min. Petrol. 138(1), 68–83.
629
630 De Hoog J.C.M., Hattori K., Jung H. (2014) Titanium- and water-rich metamorphic olivine in high-
631 pressure serpentinites from the Voltri Massif (Ligurian Alps, Italy): evidence for deep subduction of
632 high-field strength and fluid-mobile elements. Contributions to Mineralogy and Petrology 167, 990.
633
634 Deschamps, F., Guillot, S., Godard, M., Chauvel, C., Andreani, M. & Hattori, K.H. (2010). In situ
635 characterization of serpentinites from forearc mantle wedges: timing of serpentinization and behavior
636 of fluid-mobile elements in subduction zones. *Chemical Geology* **269**, 262–277.
637
638 Deschamps, F., Guillot, S., Godard, M., Andreani, M. & Hattori, K.H. (2011). Serpentinites act as sponges
639 for fluid-mobile elements in abyssal and subduction zone environments. *Terra Nova* **23**, 171–178.
640
641 Deschamps, F., Godard, M., Guillot, S., Hattori, K. (2013) Geochemistry of subduction zone
642 serpentinites: A review. Lithos 178, 96–127.
643

644 Dvir, O., Pettke, T., Fumagalli, P., and Kessel, R., 2011. Fluids in the peridotite-water system up to 6 GPa
645 and 800 degrees C: new experimental constrains on dehydration reactions. Contributions to
646 Mineralogy and Petrology 161, 829-844.
647
648 Eggins, S. M. and Shelley, J. M. G., 2002. Compositional heterogeneity in NIST SRM 610-617 glasses.
649 Geostandards Newsletter-the Journal of Geostandards and Geoanalysis 26, 269-286.
650
651 Engi, M., Berger, A. & Roselle, G.T. (2001). Role of the tectonic accretion channel in collisional orogeny.
652 *Geology* **29**, 1143–1146.
653
654 Evans, B.W. & Trommsdorff, V. (1978). Petrogenesis of garnet lherzolite, Cima di Gagnone, Lepontine
655 Alps. *Earth and Planetary Science Letters* **40**, 333-348
656
657 Evans, B.W. & Trommsdorff, V. (1983). Fluorine hydroxyl titanian clinohumite in alpine recrystallized
658 garnet peridotite: compositional controls and petrologic significance. *American Journal of Science* **283-**
659 **A** 355-369.
660
661 Evans K.A., Tomlins A.G., Cliff J., Fiorentini M. (2014) Insights into subduction zone sulfur recycling
662 from isotopic analysis of eclogite-hosted sulfides. Chemical Geology 365, 1-19
663
664 Federico, L., Crispini, L., Scambelluri, M. & Capponi G. (2007). Ophiolite mélange zone records
665 exhumation in a fossil subduction channel. *Geology*, 35 499-502.

666 Früh-Green G.L., Connolly J.A.D, Kelley D.S., Plas A. and Grobéty B. (2004) Serpentinization of oceanic
667 peridotites: Implications for geochemical cycles and biological activity. *In: The Subseafloor Biosphere at*
668 *Mid-Ocean Ridges,* eds W.D. Wilcock, D.S.Kelley, E. DeLong, C. Cary, *AGU Geophysical Monograph*
669 144:119-136.

Fumagalli, P. & Poli, S. (2005). Experimentally determined phase relations in hydrous peridotites to 6.5 GPa and their consequences on the dynamics of subduction zones. *Journal of Petrology* **46**, 555-578.

Fumasoli, M.W., 1974, Geologie des Gebietes no¨rdlich und sudlich der Jorio-Tonale-Linie im Westen von Gravedona (Como, Italia). Dissertation thesis, Zurich, Universitat Zurich, 230 p.

Gerya, T.V., Stöckhert, B. & Perchuk, A.L. (2002). Exhumation of high-pressure metamorphic rocks in a subduction channel: A numerical simulation. *Tectonics* **21**(6), 1056, doi: 1029/2002TC001406.

Harvey J., Garrido C.J., Savov I., Agostini S., Padrón-Navarta J.A., Marchesi C., Sánchez-Vizcaíno Sánchez-Vizcaíno V., Gómez-Pugnaire M.T. (2014) 11B-rich fluids in subduction zones: The role of antigorite dehydration in subducting slabs and boron isotope heterogeneity in the mantle. Chemical Geology 376, 20-30.

Hattori, K.H. & Guillot, S. (2003). Volcanic fronts form as a consequence of serpentinite dehydration in the forearc mantle wedge. *Geology* **31**, 525-528.

Heinrich, C.A. (1982). Kyanite-eclogite to amphibolite facies evolution of hydrous mafic and pelitic rocks, Adula nappe, Central Alps. *Contributions to Mineralogy and Petrology* **81**, 30–38.

Heinrich, C.A. (1986). Eclogite facies regional metamorphism of hydrous mafic rocks in the Central Alpine Adula nappe. *Journal of Petrology* **27**, 123–154.

Hyndman, R.D. & Peacock, S.M. (2003). Serpentinization of the forearc mantle. *Earth and Planetary Science Letters* **212**, 417–432,

Iwamori, H. (1998) Transportation of H_2O and melting in subduction zones. *Earth and Planetary*

698 *Science Letters* 160, 65–80

699 John, T., Scambelluri, M., Frische, M., Barnes, J. & Bach, W. (2011). Dehydration of subducting
700 serpentinite: Implications for halogen mobility in subduction zones and the deep halogen cycle: *Earth*
701 *Planetary Science Letters* **308**, 65-76.
702
703 Kendrick, M.A., Scambelluri, M., Honda, M. & Phillips, D. (2011). High abundance of noble gas and
704 chlorine delivered to the mantle by serpentinite subduction. *Nature Geoscience* **4**, 807-812.
705
706 Kessel, R., Schmidt, M. W., Ulmer, P. & Pettke, T. (2005a). Trace element signature of subduction-zone
707 fluids, melts and supercritical liquids at 120-180 km depth. *Nature* **437**, 724-727.
708 Kessel et al 2005 b
709
710 Kodolányi, J., Pettke, T., Spandler, C., Kamber, B.S. and Gméling, K. (2012) Geochemistry of ocean floor
711 and forearc serpentinites: Constraints on the ultramafic input to subduction zones. J. Petrol. 53, 235-
712 270.
713
714 Kodolanyi, J. and Pettke, T., 2011. Loss of trace elements from serpentinites during fluid-assisted
715 transformation of chrysotile to antigorite - An example from Guatemala. Chemical Geology 284, 351-
716 362.
717
718 Malaspina, N., Hermann, J., Scambelluri, M., Compagnoni, R. (2006) Polyphase inclusions in garnet-
719 orthopyroxenite (Dabie Shan, China) as monitors for metasomatism and fluid-related trace element
720 transfer in subduction zone peridotite. *Earth and Planetary Science Letters* 240, 668–680.
721
722 Marchesi C. Garrido C.J., Padrón-Navarta J.A., López Sánchez-Vizcaíno V, Gómez-Pugnaire M.T. (2013)
723 Element mobility from seafloor serpentinization to high-pressure dehydration of antigorite in
724 subducted serpentinite: Insights from the Cerro del Almirez ultramafic massif (southern Spain). Lithos

178, 128-142

McDonough, W.F. & Sun, S.-S., 1995. The composition of the Earth. *Chemical Geology* **120**, 223-253.

Möckel, J.R. (1969): Structural petrology of the garnet peridotite of Alpe Arami (Ticino, Switzerland). *Leidse Geol. Meded.* **42**, 61–130.

Nimis, P. & Trommsdorff, V. (2001). Revised thermobarometry of Alpe Arami and other garnet peridotites from the Central Alps. *Journal of Petrology* **42**, 103–115.

Pettke, T., Oberli, F., Audetat, A., Guillong, M., Simon, A. C., Hanley, J. J., and Klemm, L. M., 2012. Recent developments in element concentration and isotope ratio analysis of individual fluid inclusions by laser ablation single and multiple collector ICP-MS. *Ore Geology Reviews* **44**, 10-38.

Pfiffner, M. & Trommsdorff, V. (1998). The high-pressure ultramafic-mafic-carbonate suite of Cima Lunga-Adula, Central Alps: excursions to Cima di Gagnone and Alpe Arami. *Schweizerische Mineral. Petrogr. Mitt* **78**, 337-354.

Pluemper, O., John, T, Podldchikov, Y.Y. , Scambelluri, M. (2013) Self-organizing reactive porosity waves allow large-scale fluid escape from subducting oceanic lithosphere. Goldschmidt2013 Conference Abstracts pg. 1973

Ruepke, L.H, Phipps Morgan, J., Hort, M., Connolly, J.A.D (2004). Serpentine and the subduction zone water cycle. *Earth and Planetary Science Letters* 223, 17–34

Savov, I.P., Ryan, J.G., D'Antonio, M., Kelley, K. & Mattie, P. (2005). Geochemistry of serpentinized peridotites from the Mariana Forearc Conical Seamount, ODP Leg 125: Implications for elemental recycling at subduction zones: *Geochemistry, Geophysics, Geosystems* **6**, Q04J15, doi:10.1029/2004GC000777.

Scambelluri, M., Piccardo, G.B., Philippot, P., Robbiano, A. & Negretti L. (1997). High salinity fluid inclusions formed from recycled seawater in deeply subducted alpine serpentinite. *Earth and Planeary Science Lett*ers **148**, 485-500.

Scambelluri M., Bottazzi P., Trommsdorff V., Vannucci R., Hermann J., Gòmez-Pugnaire M.T. & Lòpez-Sànchez Vizcaino V. (2001). Incompatible element-rich fluids released by antigorite breakdown in deeply subducted mantle. *Earth and Planeary Science Lett*ers **192**, 457-470.

Scambelluri M., Müntener O., Ottolini L., Pettke T. & Vannucci R. (2004a). The fate of B, Cl and Li in the subducted oceanic mantle and in the antigorite-breakdown fluids*. Earth and Planetary Science Letters* **222**, 217-234.

Scambelluri M., Fiebig J., Malaspina N., Müntener O. & Pettke T., (2004b). Serpentinite subduction: Implications for fluid processes and trace-element recycling. *International Geology Reviews* **46**, 595-613.

Scambelluri, M., Pettke, T., and van Roermund, H. L. M., 2008. Majoritic garnets monitor deep subduction fluid flow and mantle dynamics. Geology 36, 59-62.

Scambelluri M. & Tonarini S. (2012). Boron isotope evidence for shallow fluid transfer acrosssubduction zones by serpentinized mantle. *Geology* **40**, n. 10, 907-910.

Scambelluri M., Pettke T., Rampone E. Godard M, Reusser E. 2014. Petrology and trace element budgets of high-pressure peridotites indicate subduction dehydration of serpentinized mantle (Cima di Gagnone, Central Alps, Switzerland). Journal of Petrology 55, 459-498.

779 Schmid, S.M., Rück, P. & Schreurs, G. (1990): The significance of the Schams nappes for the
780 reconstruction of the palaeotectonic evolution of the Penninic zone along the NRP20-East traverse
781 (Grisons, Eastern Switzerland). *Mémoires Societè Géologique Fr*ance **156**:263–287.
782
783 Sharp, Z.D. & Barnes, J.D. (2004). Water-soluble chlorides in massive seafloor serpentinites: a source of
784 chloride in subduction zones. *Earth and Planetary Science Letters* **226**, 243–254.
785
786 Shimizu, N., Scambelluri, M., Santiago Ramos, D., Tonarini, S. (2013). Boron and sulfur isotopic
787 variations during subduction of hydrated lithosphere: The Erro Tobbio case. *Mineralogical Magazine*
788 **77** (5), 2201.
789
790 Spandler, C., Pettke, T., and Rubatto, D., 2011. Internal and External Fluid Sources for Eclogite-facies
791 Veins in the Monviso Meta-ophiolite, Western Alps: Implications for Fluid Flow in Subduction Zones.
792 *Journal of Petrology* **52**, 1207-1236.
793
794 Spandler C., Pettke T., Hermann J. (2014) Experimental study of trace element release during
795 ultrahigh-pressure serpentinite dehydration. Earth and Planetary Science Letters 391, 296-306
796
797 Syracuse, E.M., van Keken, P.E., Abers, G.A., 2010. The global range of subduction zone thermal models.
798 Phys. Earth Planet. Int. 183, 73-90.
799
800 Tenthorey, E. & Hermann, J. (2004). Composition of fluids during serpentinite breakdown in
801 subduction zones: evidence for limited boron mobility. *Geology* **32**, 865–86
802
803 Trommsdorff, V., 1990, Metamorphism and tectonics in the Central Alps: The Alpine lithospheric
804 mélange of Cima Lunga and Adula. *Società Geologica Italiana, Memorie*. **45**, 39–49.
805

Trommsdorff, V., López Sánchez-Vizcaíno, V., Gómez-Pugnaire, M.T., Müntener, O. (1998). High pressure breakdown of antigorite to spinifex-textured olivine and orthopyroxene, SE Spain. *Contributions to Mineralogy and Petrology* **132**, 139–148.

Ulmer, P., Trommsdorff, V., 1995. Serpentine stability to mantle depths and subduction related magmatism. *Science* 268, 858–861.

Ulmer, P. & Trommsdorff, V. (1999). Phase relations of hydrous mantle subducting to 300 km. In: Fei Y, Bertka CM, Mysen BO (eds) Mantle petrology: field observations and high pressure experimentation. Special Publication No. 6. The Geochemical Society, Houston, pp 259–281

Wunder B. and Schreyer W. (1997) Antigorite: High-pressure stability in the system MgO-SiO_2-H_2O (MSH). Lithos 41, 213-227.

Figure Captions

Figure 1. Pressure-Temperature pseudosections for the Gagnone garnet peridotite (A) and chlorite harzburgite (B) (after Scambelluri et al., 2014). Arrows show possible prograde paths joining early stage assemblages, defined by monophase inclusions in high-pressure minerals, with the stability filed defined for peak eclogite-facies parageneses. Garnet peridotite in (A) records antigorite and chlorite breakdown. C: As-Sb diagram showing the array of high-pressure minerals and bulk rocks from Gagnone, comprised between Primary Mantle reservoirs and pelagic clays (after Scambelluri et al., 2014).

832 Figure 2. Textures of garnet peridotite (A and B) and of polyphase inclusions in garnet (C to F)
833 (sample MG 160 C1). Rocks contain garnet megacrystals likely representing fluid pockets in
834 garnet peridotite. F: close up of polyphase inclusions in garnet.
835
836 Figure 3. (A) and (B): scanning electron microscope images of olivine-hosted inclusions from
837 garnet peridotite and chlorite harzburgite, respectively. (A) shows an olivine reaction halo
838 between the inclusion and the olivine host. (B) shows an olivine microcrystal inside the
839 inclusion being replaced by serpentine. (c) and (D) are Mg and Si elemental maps of an olivine
840 hosted inclusion showing a continuous reaction rim of a Mg-silicate phase between inclusion
841 and host mineral.
842
843 Figure 4. Rock textures: (A) illustrates chlorite harzburgite showing an olivine +
844 orthopyroxene + chlorite + magnesite paragenesis. B shows interstitial sulphide (lower left
845 side of the picture) in between high-pressure minerals and coarse sulphide inclusion in
846 chlorite harzburgite minerals. C: primary polyphase inclusions in high-pressure olivine from
847 chlorite harzburgite. D: close up of polyphase inclsuions in olivine.
848
849 Figure 5. Elemental maps, showing element distribution inside polyphase inclusions hosted in
850 garnet. Garnet peridotite sample MG 160C1.
851
852 Figure 6. Elemental maps, showing element distribution inside polyphase inclsuions hosted in
853 olivine. Garnet peridotite sample MG 160C1, and chlorite harzburgite sample MG304 92-2.
854

855 Figure 7. Time-resolved fluid inclusion analyses. (A) is hosted by garnet, sample MG160-C1,
856 (B) is hosted by olivine, sample MG304-92-2, and (C,D) shows the same inclusion hosted in
857 olivine, sample MG160-C1.
858
859
860 Figure 8. PM-normalized trace element compositions of polyphase inclusions and of their
861 hosts in olivine (A) and garnet (B) from garnet peridotite and in olivine (C) from chlorite
862 harzburgite samples. Downward pointing arrows in (A) identify the respective limits of
863 detections for host olivine analyses. See text for implications regarding the two fluid types (A
864 in olivine and B in garnet) from the garnet perditotite.
865
866 Figure 9. Plots of Ni+Cu and S vs. Ve of of rock- and of inclusion-forming sulfides.
867
868 Figure 10. A: composition of all analysed inclusions. B: trace element patterns of Gagnone and
869 Almirez inclusions. Only reported are the element common to the two sample sets. Almirez
870 inclusion data are from Scambelluri et al. (2004b). C: trace element patterns of Gagnone
871 inclusions and of the experimental antigorite-breakdown to fluid inclusions in the P-T range
872 of 3.5-4 GPa and 700-900 °C (Spandler et al., 2014).
873
874 Figure 11. A: Mineral/fluid trace element partition coefficients (measured for fluid - host
875 mineral pairs in black and minimum KD estimated from fluid inclusion data combined with
876 mineral analyses from the same rock in grey symbols) for garnet peridotite. B: estimated
877 composition of the Gagnone garnet peridotite prior to eclogite facies antigorite dehydration.
878 The reconstructed composition only accounts for garnet and olivine, being the only phases for
879 which fluid-mineral host partition coefficients are available.

- The Gagnone metaperidotites record multistage subduction metasomatism and dehydration.
- They trap inclusions of fluids evolved during breakdown of antigorite and of chlorite.
- The trace element compositions of such fluids indicate recycling of sedimentary components
- Altered subduction-zone mantle uptakes and delivers sediment-derived elements to fluids
- This transfer process may not require concomitant subarc dehydration of slab metasediment

Figure 1

Click here to download high resolution image

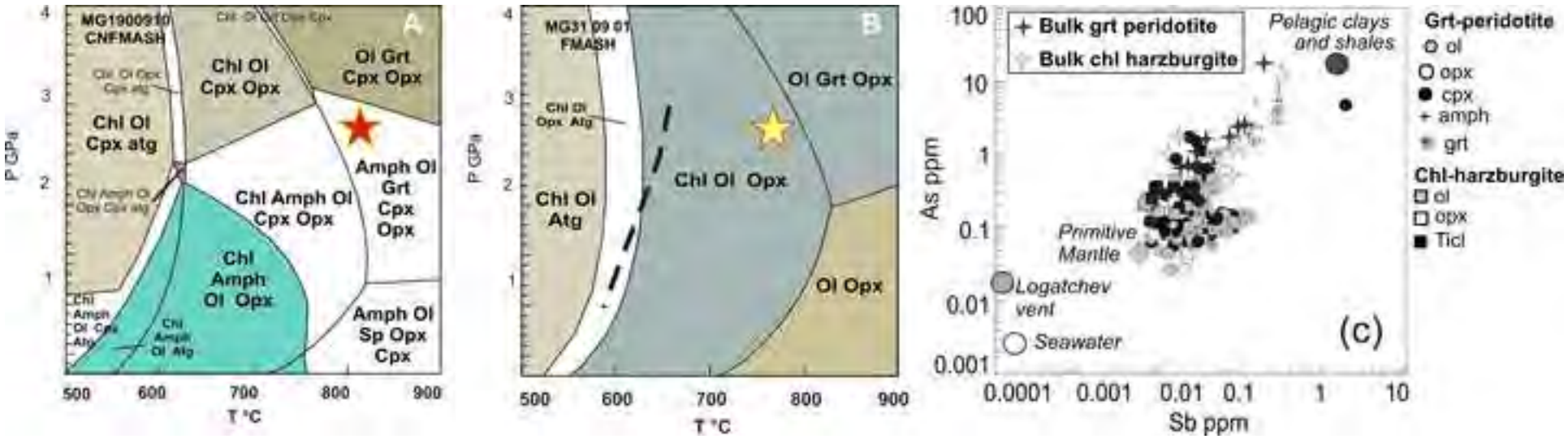

Figure 2

Click here to download high resolution image

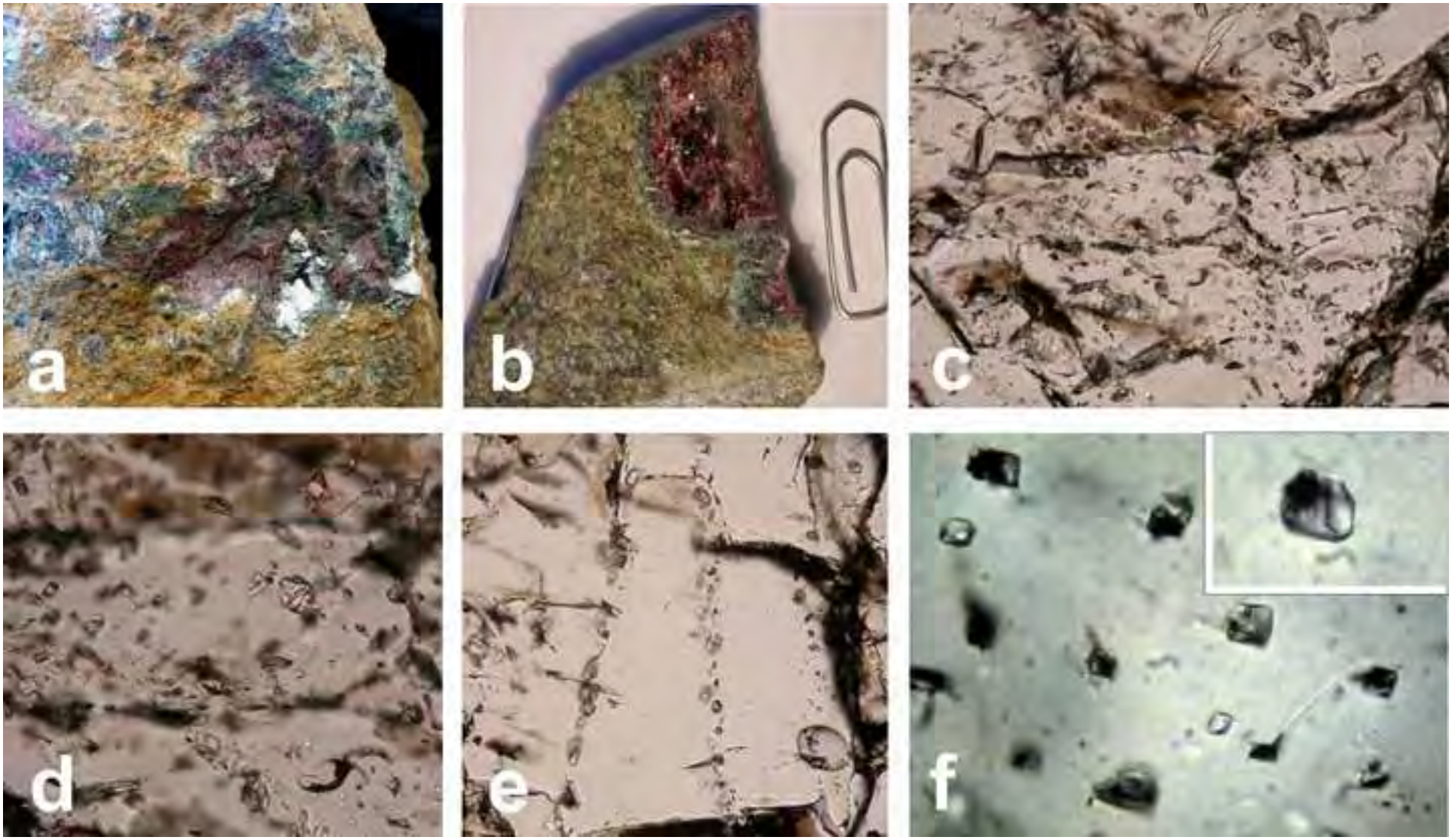

Figure 3

Click here to download high resolution image

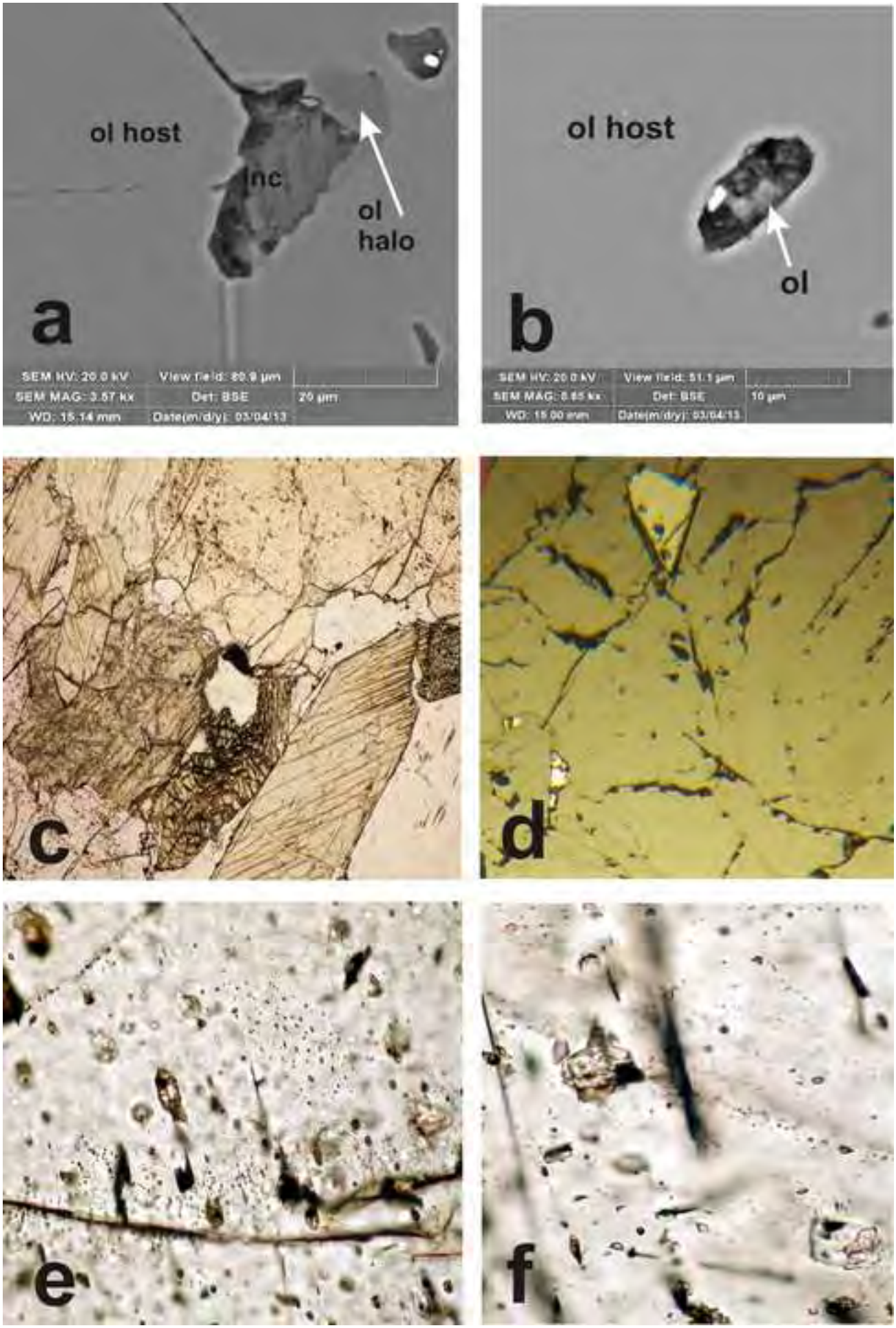

Figure 4

Click here to download high resolution image

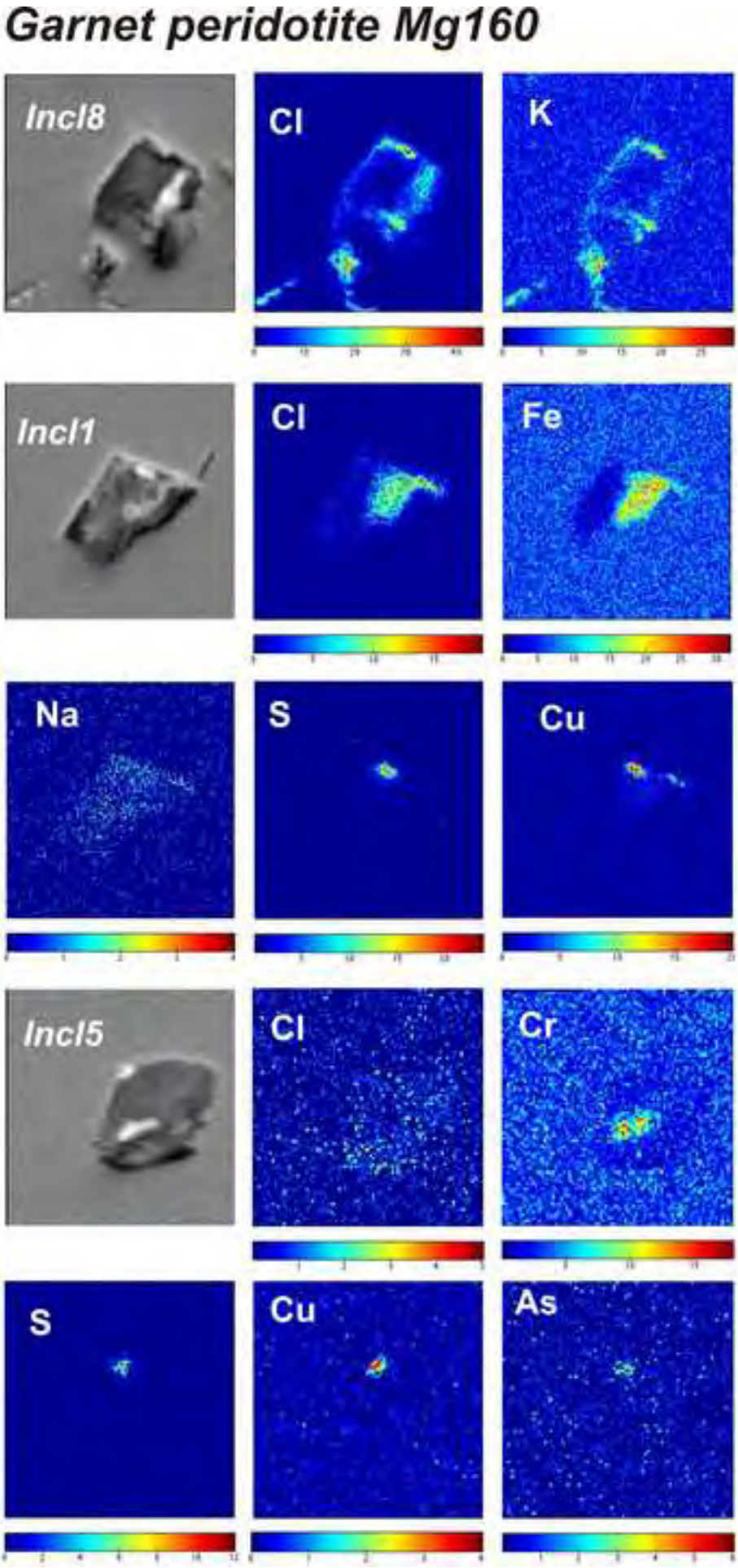

Figure 5

Click here to download high resolution image

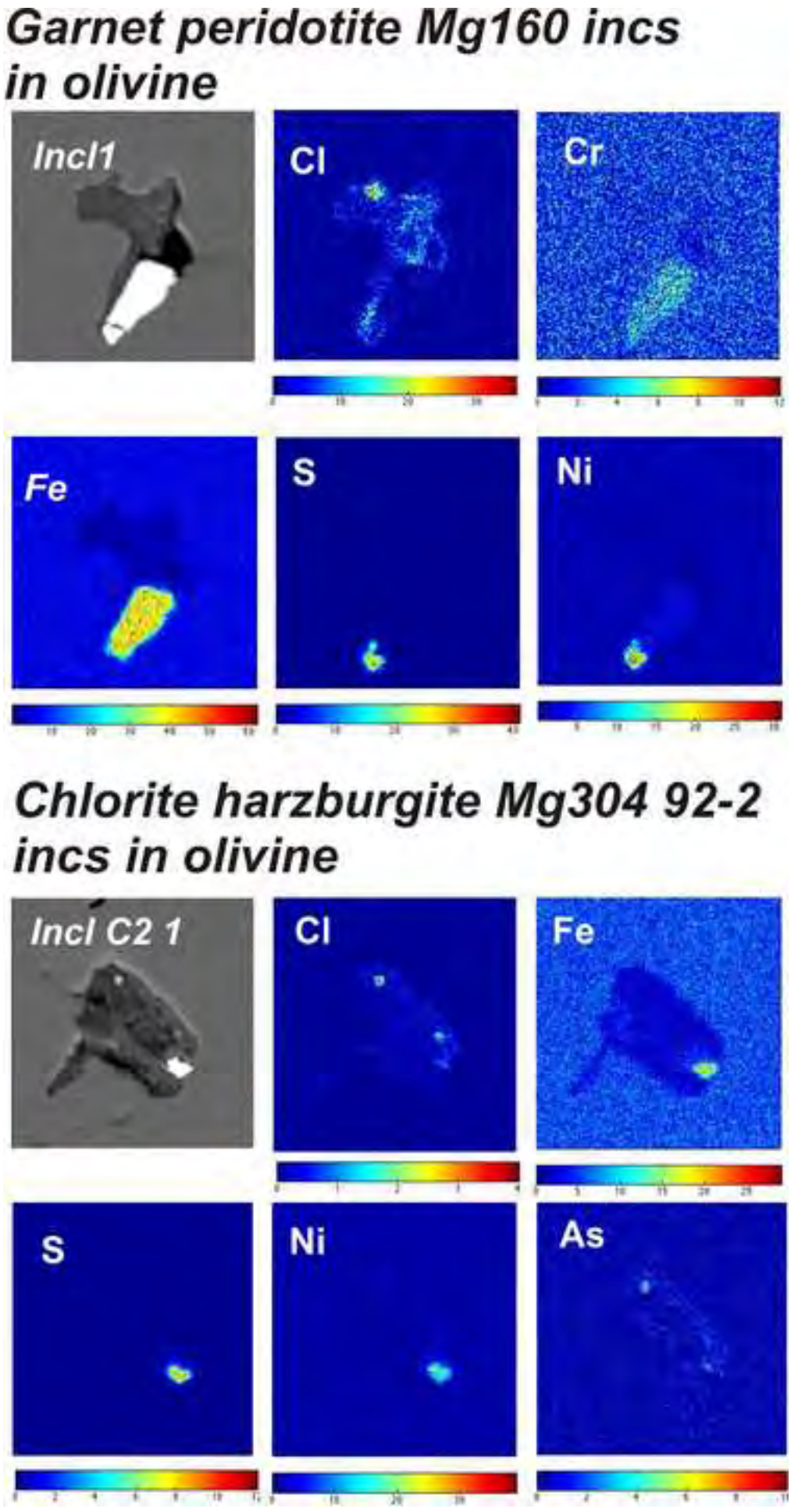

Figure 6

Click here to download high resolution image

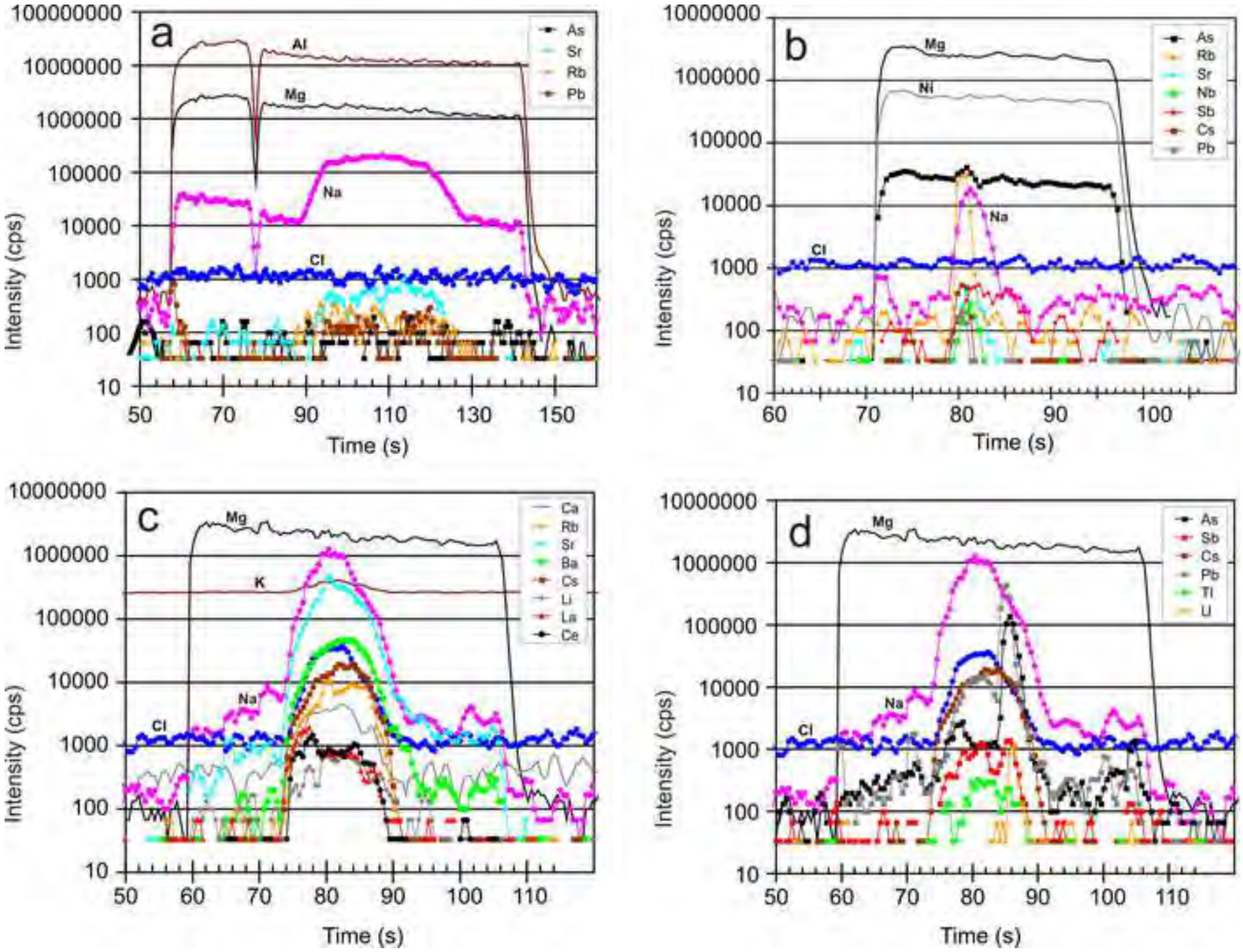

Figure 7

Click here to download high resolution image

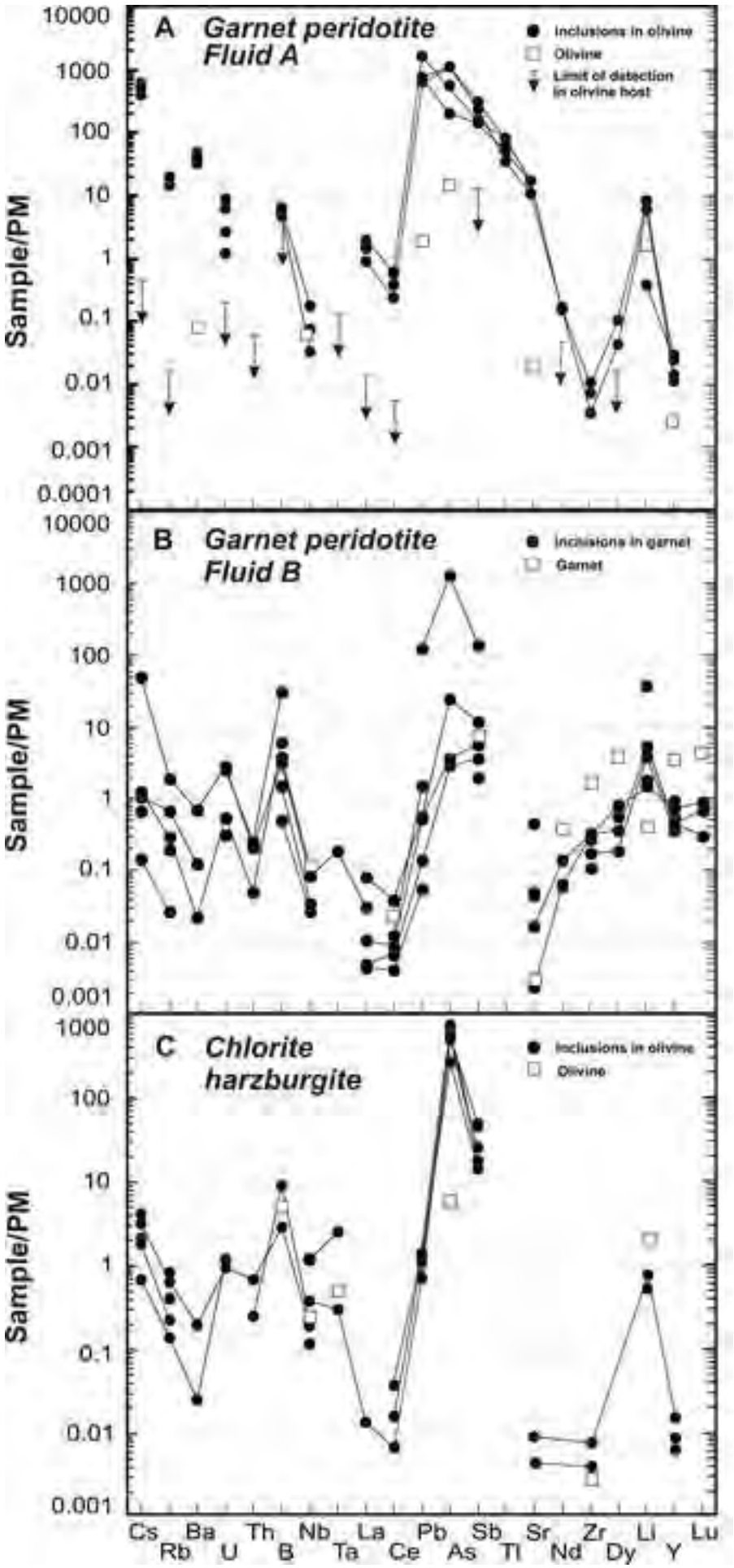

Figure 8

Click here to download high resolution image

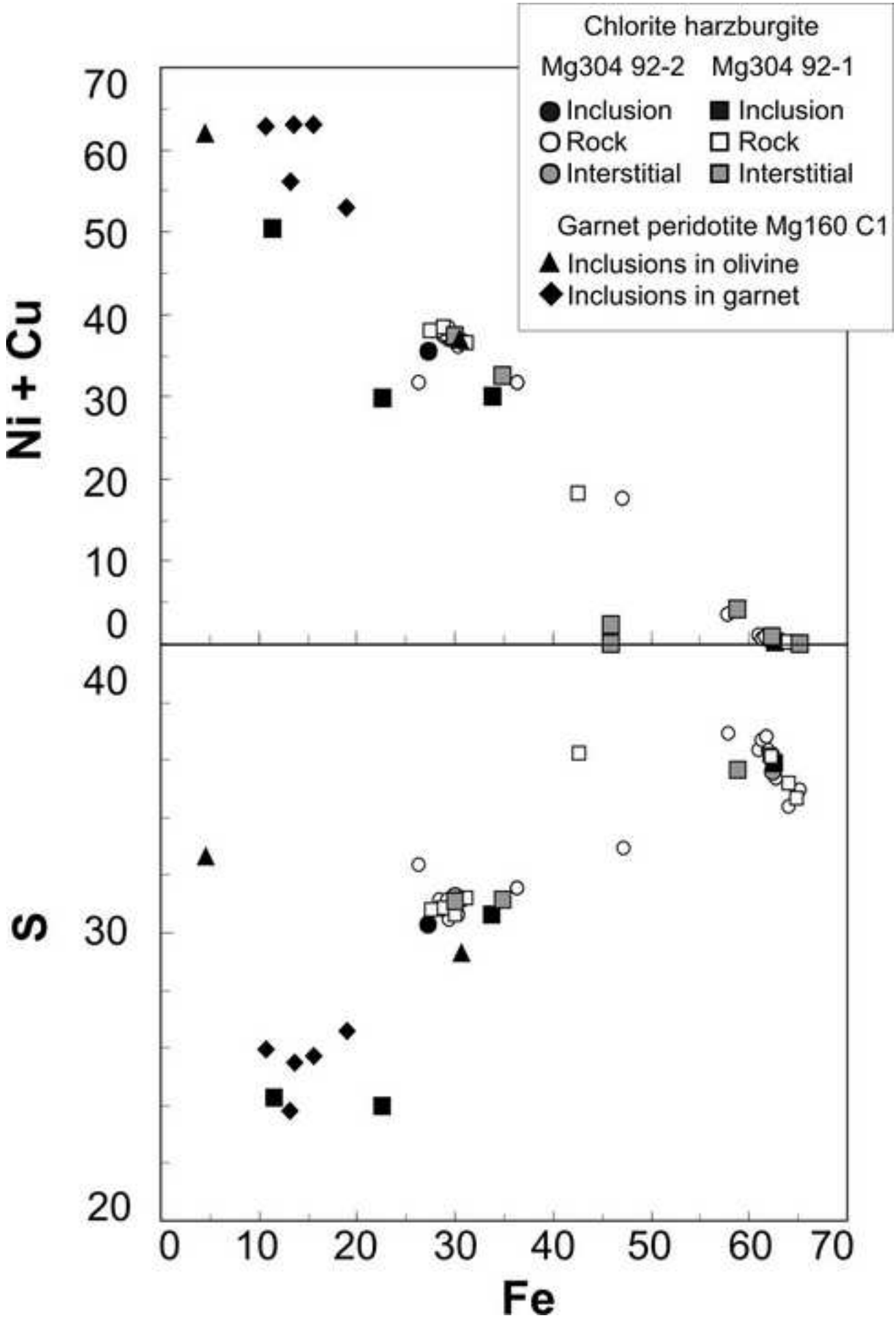

Figure 9

Click here to download high resolution image

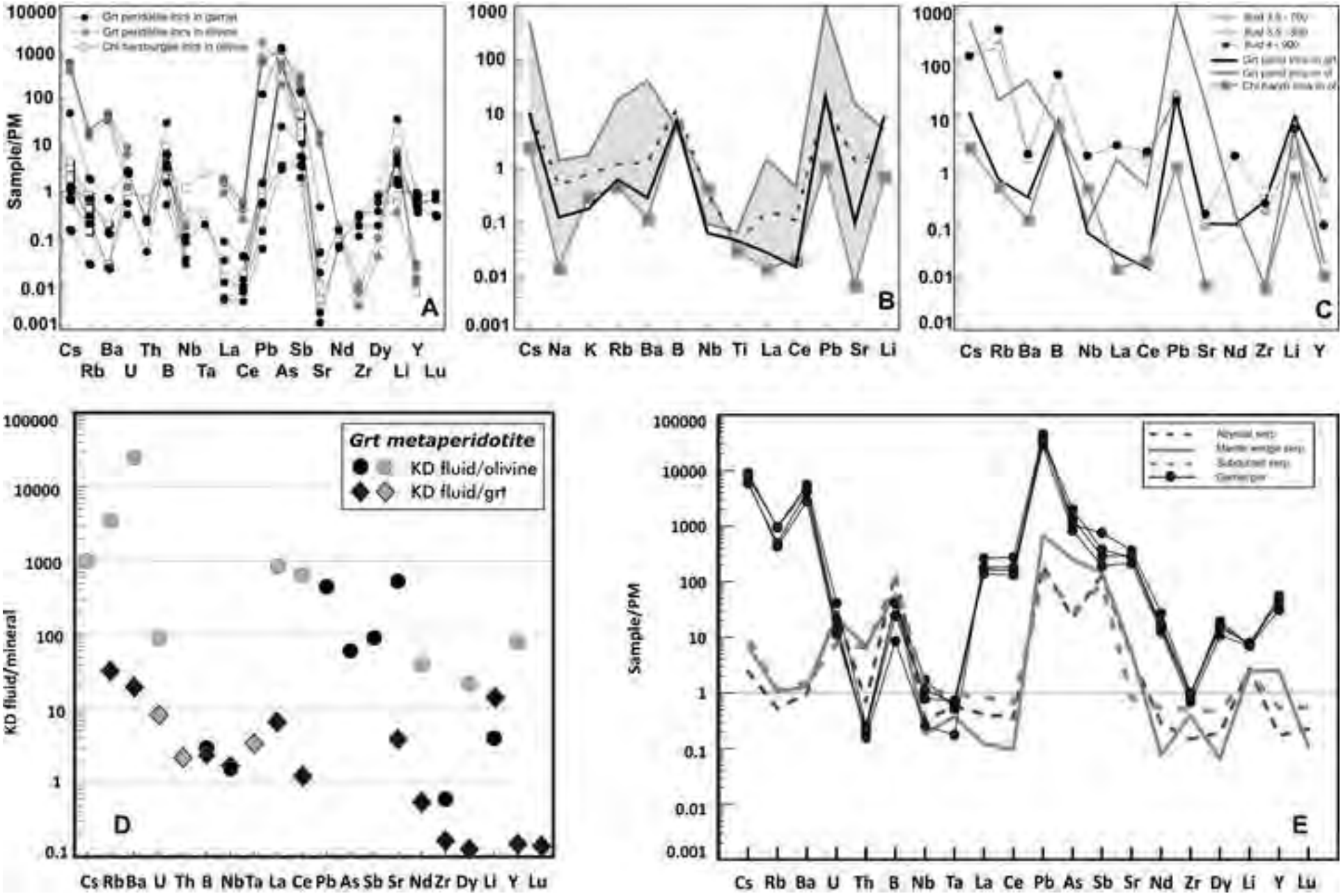

Table 1

Click here to download Table: Table 1.pdf

Table 1: LA-ICP-MS element concentration data for polyphase inclusions in garnet and olivine from Cima di Gagnone

		MG 160 C1; garnet host						MG 160 C1; olivine host					MG 304 92-2; olivine host				
Sample number		21frb04	21frb08	21frb09	21frb05	21frb06	21frb10	21frc08	21frc09	21frc11	21frc12	21frc13	21fra03	21fra11	21fra14	21fra15	21fra18
Inclusion size (µm)		40	40	55	40	55	58	25	40	22	22	18	22	60	25	25	26
	Mass																
SiO2	**29**	**10,00**	**10,00**	**9,00**	10,00	10,97	9,03	3,31	5,93	5,75	2,99	4,48	4,82	4,60	4,41	5,40	4,89
TiO2	**49**	0,0088	0,0041	0,0104	0,0105	0,0081	0,0129	0,0005	0,0124	0,0073	0,0013	0,0313	<0.0002	0,0017	0,0127	0,0089	0,0008
Al2O3	**27**	3,68	2,24	4,63	3,06	2,84	4,68	<0.0003	0,0033	<0.0006	0,0009	0,0010	0,0003	0,0025	0,0198	0,0012	0,0003
FeO	**57**	2,04	2,13	2,02	**0,17**	**0,17**	**0,17**	*<0.0004*	1,53	1,57	1,39	1,02	1,25	1,36	1,46	1,39	1,16
MgO	**25**	3,39	6,42	3,22	5,83	5,02	4,77	5,77	1,05	1,56	4,35	3,31	3,92	4,01	4,08	3,12	3,92
CaO	**43**	0,86	<0.01	1,10	0,74	0,80	1,24	0,47	0,91	0,56	0,72	0,62	<0.02	<0.008	<0.01	0,04	<0.03
Na2O	**21**	0,03	0,02	0,02	0,17	0,19	0,09	**0,50**	**0,50**	**0,50**	**0,50**	**0,50**	**0,01**	**0,01**	**0,01**	**0,01**	**0,01**
K2O	**39**	0,001	0,010	0,001	0,010	0,004	0,004	0,074	0,057	0,051	0,049	0,040	0,010	0,003	0,009	0,015	0,006
Sum		20,00	20,83	20,00	19,99	20,00	20,00	10,13	10,00	10,00	10,01	10,00	10,01	10,00	10,00	9,99	9,99
Li	**7**	2,9	*59*	2,4	8,6	6,4	8,5	9,3	11,8	0,6	8,8	12,1	<0.44	<0.10	<0.32	0,9	1,2
B	**11**	0,15	0,94	0,46	1,14	9,27	1,82	4,06	1,43	<1.50	1,95	1,84	2,69	<0.24	0,86	<1.62	<1.14
Cl	**35**	<22	800	40	<68	101	51	14100	17400	15500	14000	12600	155	43	114	<179	<131
Cr	**53**	2890	1080	2840	2620	236	2340	<7	96	<14	14	<13	<3	4	*394*	<4	<3
As	**75**	<0.02	*64*	0,1	<0.06	1,2	0,2	63	28	55	55	10	26	38	13	31	27
Rb	**85**	0,02	1,13	<0.005	0,41	0,12	0,18	8	12	9	11	12	0,25	0,08	0,39	0,50	0,14
Sr	**88**	0,03	*8,96*	0,05	0,91	0,99	0,34	170	350	220	330	340	<0.04	0,09	<0.03	0,18	<0.04
Y	**89**	2,40	4,11	3,19	1,96	1,58	1,94	0,08	0,11	0,09	0,06	0,04	0,039	0,027	0,066	<0.040	<0.037
Zr	**90**	2,77	<0.013	3,33	1,11	1,83	3,33	0,04	0,03	0,10	<0.03	0,07	<0.06	<0.01	0,04	0,08	<0.04
Nb	**93**	0,018	0,055	0,023	0,071	<0.009	<0.006	0,028	0,022	0,049	<0.02	0,114	0,149	0,255	0,125	0,792	0,077
Sb	**121**	0,01	0,14	0,02	<0.034	0,02	0,02	1,53	1,02	1,19	1,50	0,84	0,26	0,18	0,14	0,40	0,14
Cs	**133**	0,003	1,03	<0.002	0,022	0,014	0,027	4,9	12,7	8,3	11,6	10,8	0,045	0,014	0,068	0,087	0,038
Ba	**137**	<0.02	*4,6*	<0.02	0,8415	<0.04	0,149	128	320	220	290	270	<0.24	0,17	1,30	<0.32	<0.20
La	**139**	0,003	0,021	0,003	<0.006	0,053	0,007	0,33	1,25	0,59	1,05	0,94	<0.021	0,009	<0.020	<0.036	<0.028
Ce	**140**	0,007	<0.009	0,011	0,021	0,066	0,015	0,27	0,93	0,40	1,01	0,64	<0.025	0,011	0,027	0,063	<0.028
Nd	**143**	0,075	<0.06	0,083	<0.08	<0.04	0,176	<0.05	0,187	0,196	0,179	<0.14	<0.17	<0.05	<0.11	<0.13	<0.14
Dy	**163**	0,38	0,53	0,55	<0.02	0,12	0,24	0,044	0,026	<0.064	<0.056	0,064	<0.07	<0.01	<0.04	<0.10	<0.07
Lu	**175**	0,045	0,021	0,061	0,047	<0.002	0,020	n.a.	n.a.	n.a.	n.a.	n.a.	<0.016	<0.004	<0.010	<0.025	<0.015
Ta	**181**	<0.002	0,007	<0.001	<0.005	<0.002	<0.004	<0.007	<0.004	<0.017	<0.006	<0.016	<0.010	0,011	<0.013	0,092	<0.023
Tl	**205**	n.a.	n.a.	n.a.	n.a.	n.a.	n.a.	0,12	0,28	0,12	0,23	0,18	n.a.	n.a.	n.a.	n.a.	n.a.
Pb	**208**	0,009	*18,6*	0,021	0,225	0,086	0,078	61	240	95	110	112	0,16	0,11	0,19	0,21	0,11
Th	**232**	<0.001	0,017	<0.001	<0.002	0,020	0,004	0,004	<0.001	<0.024	<0.011	<0.015	0,020	<0.004	0,055	<0.034	<0.017
U	**238**	<0.002	0,064	0,007	<0.005	0,058	0,013	0,016	0,202	0,028	0,142	0,060	<0.021	0,028	0,022	<0.023	<0.017

Notes:

Element oxides are given in wt.%, elements in µg/g

Concentrations set in bold were used as the internal standard for data reduction (see text for explanations)

Entries "< value" represent limits of detection calculated for each element in every inclusion individually (Halter et al., 2002) employing the stringent LOD calculation from Pettke et al. (2012)

n.a. = not available

Values set in italic are deemed outliers and are not considered further

Note that the concentrations for Tl are to be taken with caution because Tl in SRM610 is heterogeneously distributed (Eggins and Shelley, 2002; Tl = 60 µg/g was used here)

Analytical Methods

Click here to download Supplementary material for online publication only: Repository file Analytical methods.docx

Table R1

Click here to download Supplementary material for online publication only: Table R1.xlsx

Table R2

Click here to download Supplementary material for online publication only: Table R2.xlsx

Table R3

Click here to download Supplementary material for online publication only: Table R3.xlsx

Table R4

Click here to download Supplementary material for online publication only: Table R4.xls